Thesis for the degree of Doctor of Philosophy

Contact stiffness in tyre/road noise modelling and speed dependencies of tyre/road noise generation mechanisms

Julia Winroth

Department of Civil and Environmental Engineering
Division of Applied Acoustics, Vibroacoustic Group
Chalmers University of Technology
Göteborg, Sweden, 2017

Contact stiffness in tyre/road noise modelling and speed dependencies of tyre/road noise generation mechanisms

Julia Winroth

ISBN 978-91-7597-551-1

Doktorsavhandlingar vid Chalmers tekniska högskola
Ny serie nr 4232
ISSN 0346-718X

Department of Civil and Environmental Engineering
Division of Applied Acoustics, Vibroacoustic Group
Chalmers University of Technology
SE-412 96 Göteborg, Sweden
Telephone + 46 (0) 31-772 2200

Printed by
Chalmers Reproservice
Göteborg, Sweden, 2017

Contact stiffness in tyre/road noise modelling and speed dependencies of tyre/road noise generation mechanisms

Julia Winroth
Department of Civil and Environmental Engineering
Division of Applied Acoustics, Vibroacoustic Group
Chalmers University of Technology

Abstract

Tools for simulating tyre/road noise are highly valuable in the efforts to limit the negative consequences of road traffic noise.

A numerical tyre/road noise simulation tool was in this study used to investigate how the contact stiffness parameter affects the predicted tyre/road noise. It includes a contact model with contact springs that accounts for the effect of local small-scale tread deformation. Results showed that simulated noise was sensitive to the value of the spring stiffness, primarily as it affected the total contact force. A non-linear contact spring formulation resulted in a reduction of the high-frequency content in the contact forces and simulated noise.

Aspects of small-scale tread dynamics were evaluated by simulating the detailed contact between an elastic layer and a rough road surface using a numerical time domain contact model including non-linear contact springs to account for small-scale roughness. Contact stiffness increased as the number of contact points grew as well as the deformation of their non-linear contact springs. The results imply that dynamic properties of the local tread deformation may be of importance when simulating contact details during normal tyre/road interaction conditions, but that effects of damping could, as a first approximation, be included as an increased stiffness in a quasi-static tread model.

The speed dependency of measured and simulated tyre/road noise was analysed. A large part of the noise had a high speed exponent, traditionally connected with air-pumping. However, the results showed that tyre vibrations can generate noise with a speed exponent that verges on what is expected from air-pumping. Due to the overlap in the speed exponents of the main generation mechanisms, they cannot be distinguished through a speed exponent analysis.

The most important contribution of this work is an increased understanding of how the contact spring formulation affects the simulated noise. The work has also provided insights into the speed dependency of tyre/road noise generation mechanisms.

Keywords: Tyre/road noise, Tyre/road contact modelling, Air-pumping, Speed exponent analysis, Tyre/road contact stiffness

List of publications

This thesis is based on the work contained in the following appended papers, referred to by roman numerals in the text:

Paper I
Importance of tread inertia and damping on the tyre/road contact stiffness
J. Winroth, P.B.U. Andersson and W. Kropp
Journal of Sound and Vibration 333 (2014) p. 5378–5385

Paper II
Investigating generation mechanisms of tyre/road noise by speed exponent analysis
J. Winroth, W. Kropp, C. Hoever, T. Beckenbauer and M. Männel
Applied Acoustics 115 (2017) p. 101–108

Paper III
Contact stiffness considerations when simulating tyre/road noise
J. Winroth, W. Kropp, C. Hoever, P. Höstmad (former P.B.U. Andersson)
Submitted to the *Journal of Sound and Vibration*

The following papers are not included in the thesis due to an overlap in content or a content going beyond the scope of this thesis:

Separating the contributions from air-pumping and tyre vibrations by speed dependency analysis of tyre/road noise
J. Winroth, W. Kropp, C. Hoever
Proceedings InterNoise 2016, Hamburg, Germany. p. 2158–2168, 2016

Sound generation and sound radiation from tyres
W. Kropp, J. Winroth, C. Hoever
Proceedings of InterNoise 2013, Innsbruck, Austria, p. 6252–6258, 2013

Dynamic contact stiffness and air-flow related source mechanisms in the tyre/road contact
J. Winroth
Chalmers University of Technology, Licentiate thesis, Göteborg, Sweden, 2013

The contribution of air-pumping to tyre/road noise
J. Winroth, C. Hoever, W. Kropp
Proceedings of AIA-DAGA 2013 Merano, Italy, p. 1594–1597, 2013

Numerical Modelling of Tyre/Road Interaction
P. Andersson, C. Hoever, J. Winroth and W. Kropp
Exploratory Workshop: Modern Methods of Vibro-Acoustic Studies With Automotive Applications, University of Pitesti, Romania, November 24–25, 2011

Evaluation of approximations used for the tread layer response and road surface roughness in numerical models of the tyre/road contact
J. Winroth and P.B.U. Andersson
ICSV 2011, 10-14 July 2011, Rio de Janeiro, Brazil, p. 1666–1673

Influence of tread inertia during deformation using a detailed numerical tyre/road contact model
J. Winroth and P.B.U. Andersson
Proceedings of Forum Acusticum 2011, Aalborg, Denmark, p. 2431–2434

Implementation of non-linear contact stiffness and adhesion in a numerical model for tyre/road contact
J. Winroth and P.B.U. Andersson
Proceedings of InterNoise 2010, June 13–16 2010, Lisbon, Portugal

The contribution of air-pumping to tyre/road noise.
J. Winroth, C. Hoever, W. Kropp and T. Beckenbauer
Proceedings of AIA-DAGA 2013, Merano, Italy, p. 1594–1597.

Acknowledgements

To my supervisors, Wolfgang Kropp and Patrik Höstmad: I have been fortunate to work in the vicinity of you, two strong characters with endless amounts of curiosity and drive. Your efforts and support have seen me through to this day and I am very grateful and happy.

Gunilla Skog, Börje Wijk and Camilla Gäverström have been utterly invaluable providing administrative help, technical support, and general support, thank you.

I have encountered the most brilliant, generous, and wise people throughout out my years at Applied Acoustics, including: Chiao-Ling Liao, Laura Simon, Nata Amiryarahmadi, Penny Bergman, Astrid Pieringer, Laura Estévez Mauriz, Lars Hansson, Georgios Zachos and Carsten Hoever, Alice Hoffmann, Bart van der Aa, Stig Kleiven, Anders Sköld, Onur Atak, Edmundo Guevara, Ragnar Vidarsson, Penka Dinkova, Ong Tiek Huat, Sophie Girolami, Jens Forssén, Krister Larsson, Maarten Hornikx, Tor Kihlman, Frederik Rietdijk, and Jens Ahrens. You have been such a nice bunch to encounter, motley and companionable.

A special warm cheer is here devoted to Applied Acoustics's students, former and present. It is a great comfort to have you around; your presence, banter, friendliness, and curiosity ignites sparks and brightens even the dullest of working days.

With the magical powers that will surely accompany a PhD degree, I would like to place these people in the very sweetest spot of life and sprinkle them with glittery fairytale dust while blackbirds and skylarks sing a wondrous tune: Maja Olvegård, Susanna Latos, Gustav Eek, Eija Werner, Erik Werner, Marie Lindström and Jenny Karlgren. In other words, thank you for warming my heart and having my back.

Irja Sandin, Madeleine Olsen, Natalie Bäcklund, Anna Elofsson – Thank you for reminding me that I am also part of something bigger than the acoustics academia: The real world out there with all its sunshine, hard work, and joy.

In addition, jenmc, Itsembarrassing and pinerug should be lifted, providing high-quality escape for a tired brain. And a huge hurrah for Ida L, who empowers bodies and boosts inner divas.

Without a family I wouldn't be here, for so many reasons ;-) Tack min modiga mor Inga, min kloka far Lars Fredrik, mina kära, påhittiga syskon Elof och Ru, mina älskade glädjespridare Esmeralda och Alvar + mina kusiner, kusinbarn, mina härliga mostrar, min bästa faster + Hanne + allt stöd från "the Nilssons" klanen.

Hampus, tack för att du står som en klippa i det hav där all min oro simmar ikapp. Tack för att du påminner mig om de mjuka delarna av mitt hjärta. Tack för att du får mig att tappa skallen.

Som gräshoppa, myra och svamp har jag, i stort, misslyckats. Men äldre har jag lyckats bli.

Contents

Chapter 1
Introduction

1.1 Background

Noise pollution is a growing concern and the World Health Organisation, WHO, has quantified the negative health effects of environmental noise in Europe in its report *Burden of disease from environmental noise* [1]. WHO concludes that as many as one million healthy life years are lost due to traffic-related noise in the western part of Europe each year, mainly connected with sleep disturbance and annoyance. The European Environmental Agency, EEA, reports in [2] that road traffic is the most dominant source of environmental noise. It is estimated that 125 million people in Europe are affected by road traffic noise levels greater than 55 dB L_{den} (day-evening-night level), and more than 37 million are exposed to noise levels above 65 dB L_{den}. In 1999, WHO published its *Guidelines for community noise* [3]. These guidelines conclude, for example, that the A-weighted equivalent level during daytime should not exceed 55 dB in outdoor living areas. In 2009 WHO presented *Night noise guidelines for Europe* [4], stating that the target for the A-weighted average equivalent noise level during night, $L_{night,outside}$, is 40 dB, but that an interim target is 55 dB.

Road traffic noise can be divided into propulsion noise, tyre/road noise and aerodynamic noise. The relative importance of each of these elements mainly depends on speed and type of vehicle. Tyre/road noise is created when a tyre rolls on a road. It is regarded as the main contributor to the overall road traffic noise for driving speeds above 40 km/h for passenger cars [5, 6]. Propulsion noise is traditionally considered to be most important at low velocities [5]. The development towards electric and hybrid powertrains further reduces the noise generation from this element. Aerodynamic noise, generated by the air-flow around the vehicle, is generally only considered an important contributor at very high driving speeds.

Tyre/road noise can be attributed to two main generation mechanisms: Contact forces that excite vibrations of the tyre surface, directly causing noise radiation. And a variety of small-scale air flow-related noise sources in and in the vicinity of

the contact patch, often referred to as air-pumping. Tyre/road noise typically has a broad spectrum with a peak around 800–1250 Hz for passenger car tyres, but there is great variation, as can be seen in Figure 1.1, which shows some examples of coast-by measurements of tyre/road noise [7].

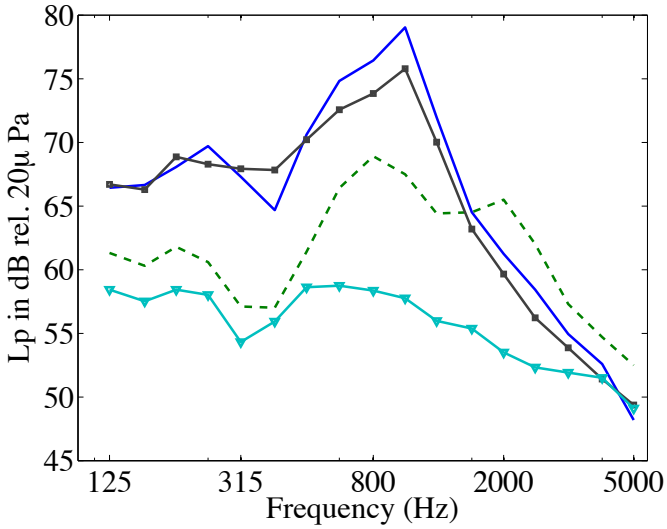

Figure 1.1: Examples of coast-by measurements of tyre/road noise for a vehicle speed around 83 km/h, adapted from [7]. Rough road–patterned tyre(–), rough road–slick tyre(–■), smooth road–patterned tyre(– –) and smooth road–slick tyre(–▼).

Measurements of tyre/road noise like those seen in Figure 1.1 contain noise from all different types of sources. One of the research problems that this thesis attempts to address is the relative importance of noise from air-pumping. It has been shown that specific air-pumping mechanisms can cause substantial noise, but there is an unsatisfying lack of understanding as to under which realistic circumstances air-pumping acts as an important contributor to in situ tyre/road noise.

Another topic of this work relates to tyre/road contact modelling in the context of tyre/road noise simulations. Simulation tools are important when trying to understand the processes that are responsible for the noise. However, to do so we need to recognise why and how the contact-stiffness parameter affects the simulated noise and what level of detail is required/suitable in the contact formulation.

1.2 Aim

One of the aims of this thesis is to increase the understanding of the contact-stiffness parameter in a tyre/road contact model and how it affects the simulated tyre/road noise. What level of detail is needed in the contact description, and what are the consequences of reducing its complexity with respect to the modelled contact forces and simulated noise?

Is the tyre/road simulation tool sufficient even when certain noise generating processes are excluded? To answer this, we need to know whether and under which circumstances the excluded sources are of significance. After tyre vibrations, air-pumping is believed to be the second most important contributor to tyre/road noise. This thesis investigates whether it is possible to extract the air-pumping contribution by studying the speed dependency of tyre/road noise.

1.3 Outline

This thesis is structured as follows.

Chapter 2 provides a review of the literature that includes tyre/road contact modelling in the context of tyre/road noise simulations and air-pumping. It also offers a description of the tyre/road noise model at Applied Acoustics that was used in the present work.

Chapter 3 includes aspects of contact stiffness in the context of tyre/road noise simulations and is based on the work with the appended *Paper I* and *Paper III*.

Chapter 3.1 contains an investigation of how the contact stiffness parameter affects the simulated tyre/road noise. (*Paper III*)

Chapter 3.2 searches for consequences of approximating what should physically be a non-linear stiffness function, with a constant value. (*Paper III*)

Chapter 3.3 covers aspects of tread inertia and damping in a very detailed tread/road contact model. (*Paper I*)

In *Chapter 4*, a speed exponent approach is applied in the effort to understand the air-pumping phenomenon and its importance for tyre/road noise. This part of the thesis is an extension of the appended *Paper II*.

Finally, the work is summarised in *Chapter 5* and future work to be done is suggested.

1.4 Limitations

Some limitations of the included work should be clarified:

The simulation of tyre/road contact forces only covers forces in the normal direction; tangential forces are not modelled. In addition, adhesive forces are not implemented.

Contact damping is not included in the contact spring formulation when modelling tyre/road noise in *Chapter 3.1–3.2*.

The contact simulations in *Chapter 3.3* and *Paper I* are limited to an elastic layer with a rigid backing indenting a 2 cm x 2 cm section of a rough road surface. Dynamic features of the belt and tread block characteristics are not covered.

Chapter 2
Tyre/road noise in the literature

2.1 Predicting tyre/road noise

Traditionally tyre vibrations are considered the main generation mechanism for tyre/road noise in the low and mid-frequency range [5]. The vibrations are excited by time-varying contact forces due to road roughness and the tyre unevenness introduced by the tread pattern. Contact forces in the normal direction may also include effects of adhesive forces that can cause the tread to *stick-snap*, see e.g. [8]. Tangential contact forces are not believed to contribute to steady-state rolling noise to any great extent, but may be of importance in specific cases and in states of acceleration. An interesting recent experimental study on frictional forces between a tread block and a road substrate can be found in [9].

Air-pumping is believed to be the second-most important contributor to tyre/road noise. It is here seen as a collection of noise sources all originating from fast acceleration of air due to the contact between road and tread during rolling.

In addition, there are various amplification mechanisms, of which the most important one is the horn effect; see e.g. [10, 11, 12]. The geometry of the tyre/road system resembles a horn-like structure, which provides a significant amplification mechanism for noise sources in, and close to, the contact patch. The horn shape gives a smooth impedance transition from the tight tyre/road contact area to the free field surrounding the tyre. The horn effect was recently addressed by Wang and Duhamel in [13], where network resonators were numerically and experimentally included in a tyre/road contact-like set-up. The results showed that the horn effect was substantially reduced at the first resonance frequency of the network.

There are different ways to approach the simulation of tyre/road noise. Physical models predict tyre/road noise by calculating each process that is involved and how they interact to produce noise. Measurement data are used as input and to validate

the models. The present work uses physical models to simulate tyre/road noise and tyre/road contact.

In a hybrid model, parts of the physical model are replaced by a statistical approach, using correlations between quantities to predict tyre/road noise. SPERoN is an example of a hybrid model, see e.g. [14, 15]. Dubois et al. [16] presented a correlation study between modelled contact forces using the Two-scale Iterative Method [17] and measured close proximity noise. They found a high positive correlation at low frequency and the results suggests that tyre/road noise levels up to the 800–1000 Hz bands can be estimated from modelled contact forces.

Even if hybrid models have been proven to be valuable from a prediction point of view, they are limited in the viewpoint of understanding as they inherently contain 'black boxes'.

2.2 Tyre/road contact in the context of tyre/road noise

To understand the tyre/road noise created by tyre vibrations, one must know the contact forces that excite these vibrations. The contact forces can then be used as input into a statistical model like [16] or into a physical model as used in the present study.

The contact between tyre and road is a non-linear system and must therefore be treated in the time domain. The non-linear characteristics come from the fact that the size of the contact patch varies during rolling. In addition, the system is nested; contact forces depend on tyre deformation, which in turn depends on the contact forces and their history.

Experimental work

Tyre/road contact is very difficult to study experimentally; the risk of altering the contact when inserting a physical sensor into the contact patch limits the possibilities. Rolling contact forces are therefore usually measured indirectly at the wheel hub, but then the results also include effects of the tyre dynamics. Due to the difficulty of studying high-frequency tyre/road contact forces experimentally, many investigations focus on developing contact models. There are, however, several successful examples of experimental work in the literature, in which dynamical contact forces are measured in the context of tyre/road noise, for example:

- Lundberg recently presented a compact internal drum test rig, designed to study the contact forces in three directions between a tread block and a substrate [9, 18]. The rig accounts for the angle of impact of the tread block and can be driven at high rolling speeds. Results are presented for a maximum rolling speed of 40 km/h. He especially notes a resemblance between his results in the tangential direction and e.g. the study of Liu et al. [19].
- Zhang measured contact forces due to rolling over idealised road asperities, both single and multiple, in [20]. A reduced-size tyre is rotated around a large concrete cylinder by a steel beam. A metallic plate, inserted in a cavity in the concrete, incorporates exchangeable asperities. Force transducers connected on the backside of the asperities indicate the contact forces when the tyre is forced to roll over the plate. Results are presented for a maximum rolling speed of 54 km/h.
- Cesbron et al. [21] measured interfacial contact forces with a matrix-based sensor where the electrical resistance of each cell was proportional to the contact pressure. The sensor was taped on different road surfaces and contact forces were measured for rolling speeds up to 50 km/h.
- Wullens and Kropp [22] validated their contact model by comparing with the acceleration measurement of a loaded tyre rolling on a rotating drum. Accelerometers were mounted and glued on the tread surface in the grooves of an airplane tyre, and good agreement was found between measured and calculated averaged power spectra of the acceleration in the normal direction.
- Andersson and Kropp [8] presented an experimental setup in which a tread sample was loaded on a road sample and then rapidly unloaded in the normal direction. It was found that the measured adherence force depended strongly on load, load duration, unloading rate, and contact geometry. The total sound pressure level of the noise generated during separation related directly to the level of the adherence force.

Local deformation

For small excitation areas, the response of a structure may exhibit *local deformation* characteristics in addition to propagating waves. Local deformation is a spring-like behaviour of the surface layer; it exists only around the excitation point and does not transmit vibrational energy into the structure. Kropp [23] made one of the first investigations of the local deformation of tyres by measuring driving mobilities using different excitation areas. Local deformation of tyres was later also nicely shown by Andersson et al. [24], who found it both in mobility measurements and

in the results of the numerical two-layer model by Larsson and Kropp [25]. One important conclusion of their work was that high-frequency mobility measurements on tyres are strongly affected by the excitation area. The effect can even be seen at low frequencies for very small excitation areas. Figure 2.1 shows measured and modelled radial point mobility for different excitation areas. At low frequencies, the mobility is dominated by rigid body modes together with the first circumferential modes. The first cross-sectional modes generally cut in at around 300–400 Hz. The two broad peaks, around 350 Hz and 550 Hz in the figure, are in [26] explained as results of groups of modes with the same cross-sectional order but different orders in the circumferential direction. At high frequencies, individual modes or groups of modes become difficult to distinguish. The response of the tyre resembles more that of an infinite plate in addition to the influence of local deformation. A conclusion from [24] was that high-frequency tyre models must include the local deformation to be able to simulate the contact behaviour of the tyre at these frequencies.

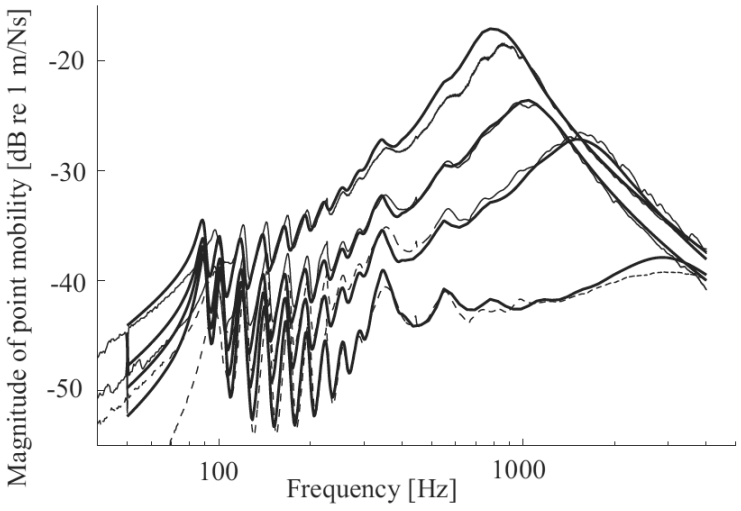

Figure 2.1: Figure from [24], included here with permission from the author. Radial point mobility for a smooth tyre excited in the middle of the tread using four different excitation areas: calculated with excitation areas (all in millimetres) 2×2, 4×4, 6×6 and 15×15 (from top downwards in solid lines) and measured with excitation areas of a radius of 2.3 mm, 4.5 mm, 6.9mm and 15 mm$\times$15 mm (from the top downwards in dashed lines).

Tyre/road contact modelling

A perfect tyre model and a perfect description of the road, including a significant spatial resolution, would not require any additional contact model. Unfortunately, no such model can be found in the literature. Larsson [25] suggested an analytical two-layer tyre model based on the elastic field equations. Although this model could predict local deformation correctly [24], it suffers from a simplification of the geometry, as it considers the tyre to be a flat plate. Hence the *contact* was found to be correctly captured but the *tyre dynamics* not so well.

Models based on numerical approaches such as Finite Elements (FE) (e.g. [27, 28, 29, 30]) can be found on the other side of the *correct contact* versus *realistic tyre response* scale. Such tyre models will always suffer from a limited spatial discretisation, which reduce their potential to predict the local deformation with sufficient accuracy. By using a wave guide finite element (WFE) approach, the spatial discretisation can be increased and/or the computational effort reduced, see e.g. [31, 32, 33, 34, 35, 26].

A common approach to tyre/road interaction is to use a adequate tyre model that is able to capture the dynamics of the tyre structure, in combination with a contact model. The latter typically introduces a third medium between the tyre model and the road description, which includes the effects of local deformation when individual road asperities intrude into the tyre tread. How much of the tread dynamics is included the contact model depends on the level of detail of the tyre model.

Different types of contact models can be found in the literature; one common method is to use a set of isolated ideal springs, "Winkler bedding"-models (e.g. [36, 37, 38, 39, 40]) or elastic half-space approaches (e.g. [22, 41, 17, 16, 42, 20]).

The elastic half-space includes local deformation and coupling between tread elements. However, it has some limitations, e.g. it assumes that the contact area is small compared to the dimension of the body. And without the introduction of inertia and/or viscoelasticity it assumes infinite wave speed and a single, frequency-independent value must be approximated for the stiffness. Wullens and Kropp [22] used an elastic half-space to model the tread and noted that the shortcomings of the approach were compensated for by updating the Young's modulus parameter of the half-space. The value of the stiffness was found by evaluating the average contact area, which is an approach used in many studies.

Zhang [20] found a good agreement between measured and modelled maximum contact force when a pneumatic tyre rolls over a single asperity when using a "carefully calibrated Young's modulus" of the elastic half-space. He also noted that viscoelasticity is needed in the model to simulate the asymmetry in the time

development of the contact force found in the measurements. Viscoelastic effects were also included in the work of Dubois et.al. [43]. The interesting work by Liu et al. [19, 44] shows that the contact force increases with indentation speed due to the viscoelasticity of the tread rubber. A similar conclusion is found in the present work, Chapter 3.3 and in Paper I. Contact models that include energy losses in within the tread are otherwise more often found in studies where rolling resistance is the main focus, e.g. [45, 46].

Contact stiffness formulations

A numerical tyre/road interaction model must employ spatial discretisation of the contact. The question arises of how to handle surface roughness on smaller length scales than the spatial resolution, i.e. the roughness within the elements. One approach is to neglect this information and basically 'flatten' the surface of each element. However, this results in an overestimation of the contact stiffness as the contact initialises at a limited number of small-scale contact points. An increasing number of small-scale contacts form as the indentation grows. Eventually the small-scale contact reaches saturation as no new small-scale contacts are formed. The stiffness of the contact is then solely determined by the response of the tyre model (if the road is considered rigid).

In other words: The area of real contact is substantially smaller than the apparent contact area; what looks like complete contact within an element with one specific spatial discretisation will, at a finer resolution, consist of less total contact area. Consequently, the contact will be softer than can be expected from the apparent area of contact.

Non-linear contact springs whose stiffness increases with increasing spring deformation can be used to approximate the effect of an increasing number of small-scale particles making contact within an element. Assuming a *constant* stiffness value of the contact springs has been shown to be a successful simplified approach, applied by e.g. Hoever [26]. The force-indentation curve must then be linearised at a specific working point to find this value. Hoever reported a good match between simulated and measured truck tyre/road noise in [26]. The stiffness of the contact springs was updated to match the modelled static footprint with measurements. This procedure is used very often, but it was noted in [39] that the contact spring stiffness was at least partly tuned to compensate for a less accurate side-wall stiffness.

Finding a single value for the contact stiffness is a delicate problem and it is not self-evident that it is more straight-forward to estimate a non-linear stiffness

function. Despite the difficulties, some approaches for determining the non-linear contact stiffness of tyre/road interaction have been suggested in the literature.

Gäbel [47] found the non-linear stiffness function of a tread-rubber block indenting a road surface by adding contributions from very many springs with constant stiffness, distributed according to a cumulative height-distribution function specific to each road surface. The stiffness of the springs was found through comparison with measurements. Andersson and Kropp [48] also used non-linear stiffness functions in their very detailed tread block/road contact model. For the smallest length scales, they applied a model of a circular punch indenting an elastic layer, taking into account the increase in contact area with increasing load. Paper I includes an extension of the model that includes damping and inertia in the tread model that couples the non-linear springs. It suggests that at least the stiffening effect of damping should be accounted for in a tread/road contact model.

The small-scale contact model presented in [48] has also been used in the context of modelling rolling resistance by Artega [46] and Boere et al. [49].

Persson has been involved in analytical efforts to find the right stiffness function of a tread block indenting a road surface, see e.g. [50, 51]. The strain dependency of the rubber's Young's modulus must be considered, as well as assumptions of the fractal dimensionality of the road surface. Good agreement with measurements was found for many different road surfaces in [51]. Pinnington [52] used a particle–envelope model to describe roughness on several different length scales when modelling tyre/road contact.

Figure 2.2 illustrates the general idea of an approach that is used in Chapter 3.2, inspired by [47]. The figure shows an example of a discretised road contour and its height distribution, which describes how many road elements, N, can be found at or above a certain height, z. As a tyre tread is pressed into a road surface, an increasing number of surface point come into contact. It is assumed that the stiffness characteristic is directly proportional to the number of points in contact and hence comparable to the height distribution curve in Figure 2.2. This function will have a somewhat steeper rise with indentation than in reality, as it neglects the deformation of the tread. This deformation could potentially keep contact elements from making contact at each given indentation depth.

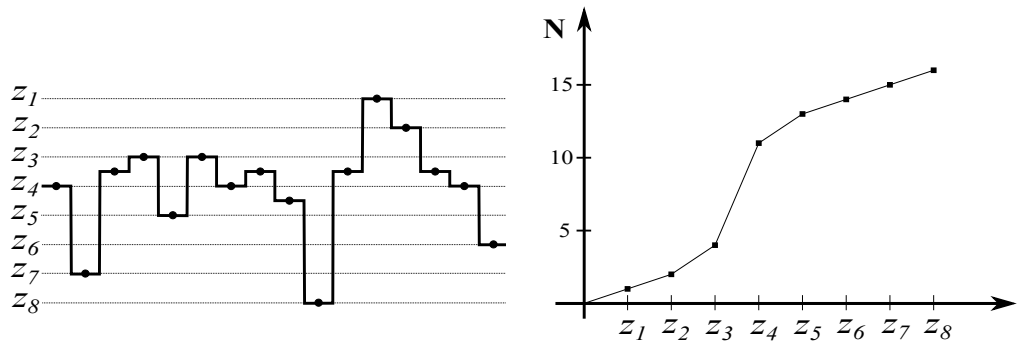

Figure 2.2: Example of a discretised road surface (left) and its height distribution (right): For each road height z, the number of points at or above this height, N, is plotted against z.

Effects of contact stiffness on modelled tyre/road noise

The contact stiffness formulation affects the size of the contact patch, as reported in several studies in the literature. However, there is a lack of investigations showing the effect on the contact forces and radiated noise.

Wullens and Kropp found in [53] (results also briefly reproduced in [5]) that the choice of local contact stiffness of the rubber in the model proposed by Kropp [23] had a great effect on the spectrum of the modelled total contact force and averaged noise generation of the simulated belt vibrations. The tyre model used was an orthotropic plate on an elastic foundation, discretised into lateral slices along the circumference, and the local stiffness of the tread rubber was represented by springs with constant stiffness.

Study [54] also showed that the choice of contact stiffness has a great effect on the resulting simulated noise; stiffer contact springs increased the sound pressure level, especially above 1000 Hz. The average total contact force was found to be unaffected by contact stiffness changes. This could be expected due to the model's interaction conditions; a predetermined load is applied in an initial phase and the obtained steady state distance – "tyre rim-road" – is maintained during the rolling phase. The spectra of contact forces, on the other hand, showed a contact stiffness dependency; however it was slightly difficult to interpret. It was also speculated that the high sensitivity of the simulated sound pressure level could be related to differences in tyre deformation affecting the strength of the horn effect.

2.3 Air-pumping

Presented in the following is an overview of *some* of the work that has been done in the endeavour to model and understand air-pumping noise. It does not claim full coverage; rather, a few of the interesting works are investigated in greater depth. A literature study also covering resonance phenomena in tyre/road contact can be found in e.g. [55].

One of the first researchers to introduce air-pumping as an important concept in tyre/road noise was Hayden in 1971 [56]. His idea was that noise is generated when air is forced to move rapidly in the contact zone during rolling: First being pressed out of voids in the tread or cavities in the road where the tread meets and deforms to the road, and then sucked in where the tread leaves the contact. These types of fluctuations in volumetric air-flow rate constitute the basics for the acoustic monopole source and the mean squared acoustic pressure at a distance r from such a source, $\overline{p^2}(r)$, is given by:

$$\overline{p^2}(r) = \frac{\rho}{16\pi^2 r^2}\overline{\left(\frac{\partial Q}{\partial t}\right)^2}\,, \tag{2.1}$$

where ρ is the density of the medium, and Q is the volumetric flow rate from the source. The time derivative of Q is given as $j\omega Q$ assuming harmonic motion and Equation 2.1 can be written as:

$$\overline{p^2}(r) \approx 2 \cdot 10^5 \cdot \left(\frac{\omega^2 \overline{Q^2}}{r^2}\right) \tag{2.2}$$

Hayden used this formula to estimate the total sound pressure level of a tyre with tread cavities giving rise to these types of monopole sources at the leading and trailing edge, rolling on a smooth surface. The characteristic frequency was identified to be the occurrence of the flow pulses: $\omega \approx 2\pi V/S$ where V is the forward velocity and S is the circumferential distance between tread cavities and with this the sound pressure level can be written:

$$Lp = C + 40 \cdot \log_{10}(V) - 20 \cdot \log_{10}(r)\,, \tag{2.3}$$

where C is a factor that depends on the tread depth, width of the cavities, fractional change of the volume of the cavities during contact and the number of cavities per unit width of the tyre. Despite the modesty of the model, e.g. the assumed omni directionality of the noise sources, Hayden found agreement with tyre/road noise measurements, especially for the predicted speed dependency.

In the following decades, his ideas were investigated by others; e.g. Plotkin et al. found experimental support for Hayden's air-pumping model [57]. Ronneberger

presented another idea of how air is forced to move when an elastic half-space indents ideal road asperities, also producing monopole-like sources [10].

Where Hayden imagined that air is rapidly being expelled in the leading edge of the contact when the tread deforms (and vice versa in the trailing edge), others have argued that air-pumping noise exists without tread deformation. In these cases, the rolling motion of the tyre is considered to drag the air boundary layer around the tyre into the contact, creating an overpressure in the leading edge. The motion of the tyre then seals air pockets with this over-pressure that is being released at the trailing edge, see Figure 2.3 taken from [58].

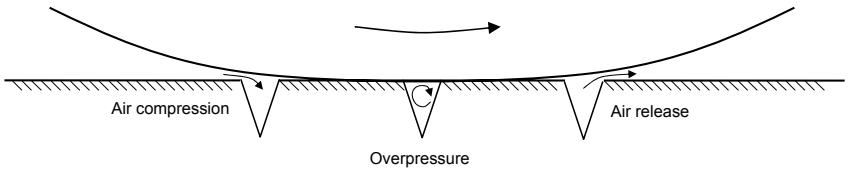

Figure 2.3: Idea of air-pumping presented in [58].

Hamet et al. [59] showed in experiments that openings in the form of cylindrical cavities in an otherwise smooth road surface generate strong noise when they are run over by a slick tyre. It was found that noise mainly radiated at the trailing edge when the cavity that had been under pressure during contact was opened. The noise created at the trailing edge could relate to the idea of 'air resonant radiation' as proposed by Nilsson in 1979 [60].

Conte and Jean studied air-pumping noise due to the compression of air, closing of cavities and opening of cavities in the tyre/road contact patch using a computational fluid dynamics (CFD) model [61]. The case with a single cavity was compared with the experimental work of Hamet [59] and there was good agreement between the CFD calculations and the experiments considering that the calculations were done in 2D and that tread deformation penetrating the cavity was not taken into account. Later, Conte extended the model to 3D [62] and included the effect of lateral porosity due to road texture [63]. The latter was shown to reduce the influence of the previously dominating Helmholtz resonance created when the over-pressurised road cavity opens as it exits the contact patch. He emphasised the importance of the turbulence model used and the detailed shape of the tyre surface near the contact patch.

Gagen [64] argued that linear acoustic theory is incorrect for tread groove squeezing during tyre/road contact. Kim et al. [65] adopted the ideas of Gagen and used a hybrid technique including CFD and a Kirchhoff integral method for the generated

far-field sound. It was concluded that the very high-frequency noise (2–8 kHz) increased when the non-linear type of source was used.

The number of air-pumping mechanisms that have been suggested and tested theoretically, experimentally, and numerically, could be taken as an indicator in itself that there is a contribution of this kind of noise source to real tyre/road noise. This is of course a vague argument; very few of the cases found in the literature can be connected to real tyre/road interaction situations. In fact, when Conte made his CFD model more realistic by including lateral porosity, the sound radiation drastically changed and decreased [63].

Correlation studies of e.g. road spectrum and tyre/road noise [5], or modelled contact forces and tyre/road noise [16], have been interpreted to indicate that a part of the noise can be attributed to air-pumping and that this is a high frequency phenomenon, approximately above 1000 Hz. One objection to this conclusion could be the disregard of the contact filter effect, which decouples tyre excitation from the amplitude of surface roughness with wavelengths much smaller than the contact length.

Heckl concluded in 1986 that Hayden's air-pumping theory is unable to explain tyre/road noise except in special cases [66], but in the same paper he noted that results obtained with Ronneberger's air-pumping theory (see e.g. [10]) agree with measurements for frequencies above 600 Hz. Heckl also promoted the idea that the radiation efficiency of vibrational modes on a tyre are of great importance for tyre/road noise generation. Kropp et al. [35] showed that mainly low-order modes with eigenfrequencies in the low frequency range determine tyre/road noise in a wide frequency range, all the way up to 2 kHz. They concluded that one possible explanation could be that the radiation efficiencies of these modes make them very important even if they are driven in a frequency range far from where they have their maximum amplitude. The complex tyre/road noise model used by Kropp was further developed by Hoever, who showed that tyre/road noise can be accurately predicted, even above 1 kHz, by a model that only considers tyre vibrations – aerodynamic sources are not incorporated [40, 26]. However, the investigation presented in Chapter 3 and Paper III indicates that some of the contribution in the high frequencies of the simulated noise may be due to the choice of a constant stiffness of the contact springs used in the model.

2.4 Influence of vehicle speed on tyre/road noise

The acoustic pressure of tyre/road noise, p^2, is commonly found to be proportional to the vehicle speed, U, to the power of a constant speed exponent, k:

$$p^2 \propto U^k \tag{2.4}$$

One way to assess the mechanisms involved in the creation of tyre/road noise could be to study how the noise depends on the vehicle speed. A prerequisite is that the expected speed exponent for each noise source mechanism is known and not overlapping each other. Hayden's theory of air-pumping noise resulted in a U^4 relationship for the total sound pressure level as seen in Equation 2.3. This relationship holds true in general for acoustic monopole sources. Conte found e.g. a speed exponent of 3 for the noise created in front of the tyre in his two-dimensional CFD air-pumping model [67]. This would correspond to a speed exponent of 4 in three dimensions according to Heckl [68]. The next order, U^6, is expected for dipole sources, e.g. the noise created from periodic vortex shedding by the wind flow around an object. It is more complex to estimate the expected speed dependency of the sound radiation caused by vibrations of a structure like a tyre. In general, the radiated sound power is proportional to the rms-surface velocity to the power of two, but strictly one must also consider the radiation characteristics of the structure.

Even though the speed dependency of tyre/road noise has been investigated and commented on in the literature, no deeper analysis has been presented. A high speed exponent is usually taken as an indication of air-pumping and a low speed exponent is taken as an indication of tyre vibrations. This may be correct as a 'rule of thumb', but issues with the pitch of the tread pattern or wind noise, could make the conclusions less accurate. In a review paper from 1986, Heckl [66] referred to experiments showing that the radiated sound power from a tyre was proportional to the rolling speed raised to the power of 3–4. The report from the Sperenberg project, [7], stated that the expected speed exponent for radial vibrations of the tyre carcass is 2.0–3.0 and that air-pumping mechanisms are expected to have 4.0–5.0. During the work with designing the semi-statistical model SPERoN (see e.g. [14]), a speed exponent of around 4 was found surprisingly often in most third octave bands for slick tyres. This was interpreted as a strong influence of noise generated by air-flow related sources. Paje et al. [69] presented A-weighted close proximity measurement data from a patterned passenger car tyre on a conventional porous road surface. They investigated the speed exponent for the overall level as well as for the third-octave bands between 300 Hz and 4 kHz. They claim to see a higher

speed exponent in the higher frequency bands and take this as an indication of air-pumping. However, looking more closely at how the speed exponent varies with frequency in the presented data, one can see that it is close to 4 even for the lowest bands, then it drops to below 2 around 630 Hz, to again rise to around 4 above 1000 Hz. Even if not commented, a possible explanation for the dip in the speed exponent curve at the mid-frequencies could be related to the pitch effect of the tread pattern.

Oswald [70] investigated aerodynamic vehicle noise and suggested that it could be the most important component above 80 km/h for lightweight vehicles with slick tyres. The study also showed that wind noise has a strong front-vehicle directivity. A similar finding was made in [7], where wind tunnel measurements showed that wind noise has a strong influence and can dominate the measured coast-by noise for quiet tyre/road combinations. Anfosso-Ledee and Kragh [71] found less influence of wind noise in CPX measurements for test vehicle speeds up to 90 km/h but they recommended to consider results below 400 Hz and above 4 kHz with care.

Another potential problem with speed exponents in tyre/road noise literature is the tendency to study A-weighted levels. This becomes especially troublesome when strong pitch effects are expected (e.g. tread pattern on smooth roads), as in such cases noise energy is transferred between frequency bands with different weighting when driving at different speeds.

2.5 The tyre/road noise simulating tool at Chalmers

The tyre/road noise model that was utilised in this work was developed and improved by the tyre/road noise group at Applied Acoustics, Chalmers University of Technology (e.g. [72, 73, 74, 34, 26]). It is built around three modules: a tyre model, a contact model, and a radiation model. Together, these form a cogent, flexible tool for simulating tyre input and transfer mobilities [75], rolling noise [35] and rolling resistance [45]. It has been shown to accurately capture the horn effect, see e.g. [35] where calculation results were compared with measurements presented in [12], showing good agreement. Recently, the tyre/road interaction model has been extended to include the tyre air cavity and the corresponding structural–acoustical coupling [76]. However, in the present work a more fundamental version of the simulation tool is used, which does not include the air cavity and energy losses in the contact model.

2.5.1 Tyre model

The present tyre module is constituted of a waveguide finite element model (WFEM) that describes the dynamical behaviour of the tyre. It provides the time-domain Green's functions that are used as input to the contact module and it calculates the tyre surface vibrations resulting from the tyre/road interaction, which are then input to the radiation module.

A modal approach is possible when using proportional damping in the WFEM. In this case, the vibrational field on the tyre is composed of cross-sectional modes combined with waves propagating in positive and negative directions around the tyre. Only discrete wave numbers can exist in the circumferential direction, corresponding to integer multiples called polar orders (denoted *n*).

Equation 2.5, adopted from [35] describes the total vibrational field on the tyre at the angular coordinate θ, $\mathbf{V}(\theta, \omega)$ as a summation of the contribution of Q cross-sectional modes in combination with Γ circumferential waves travelling in the positive and negative direction respectively. The eigenfunction $\mathbf{\Psi}_{n,i}$ represents the cross-sectional mode i expanded along the circumference as a wave with polar order n [45]. $\mathbf{F}_n$ is a modal expansion of the excitation force. The resulting modal amplitudes are given as $A_{n,i}$ and $B_{n,i}$ in Equations 2.6 and 2.7.

$$\mathbf{V}(\theta, \omega) = \sum_{n=0}^{\Gamma} \sum_{i=1}^{Q} (A_{n,i}(\omega)\mathbf{\Psi}_{n,i}\, e^{jn\theta} + B_{n,i}(\omega)\mathbf{\Psi}^*_{n,i}\, e^{-jn\theta}) \tag{2.5}$$

$$A_{n,i}(\omega) = \frac{\mathbf{\Psi}^{*T}_{n,i}\, \mathbf{F}_n(\omega)}{q(\omega)} \tag{2.6}$$

$$B_{n,i}(\omega) = \frac{\mathbf{\Psi}^{T}_{n,i}\, \mathbf{F}_{-n}(\omega)}{q(\omega)} \tag{2.7}$$

where ω is the angular frequency and the denominator is here consolidated into a function $q(\omega)$ that depends on eigenfrequency, angular frequency and damping. When n = 0, the amplitudes in Equations 2.6 and 2.7 have to be divided by two. The interested reader will find thorough descriptions and discussions about the tyre WFEM in e.g. [75, 26, 45, 35].

2.5.2 Contact model

The contact model delivers the contact forces during rolling. The forces are determined by the condition that the tread must deform due to the static load and the time-varying penetration of roughness asperities. Vibrations of the tyre structure as well as the local deformation in the tread can be calculated from the contact forces.

A number of tracks containing scanned road texture data are used in the contact calculation. In [77] it was shown that at least 5–6 tracks are necessary to get an accurate representation of the road in the contact calculation; in the present work 10 tracks are used. The roughness within each contact element is approximately taken into account using contact springs. When a tyre tread element first makes contact with a road element in the contact calculation, the contact is actually partial and the effective contact stiffness is less than the bulk material stiffness due to effects of local deformation. The implementation of contact springs with constant stiffness in the tyre/road interaction model used in this work is well described in e.g. [45].

The contact calculation starts with a loading phase where the tyre is slowly lowered onto the road until the prescribed total static contact force is reached. The distance between the rim and the road is then noted; this distance is kept fixed when the tyre starts rolling.

The contour of an undeformed tyre (defined by the fixed rim–road distance) enters each rolling time step as a boundary condition to the contact calculation where the contact forces and their spatial distribution are sought. Figure 2.4 shows a schematic view of the detailed contact at one time instance, zoomed to a few contact points.

The contact is set up in such a way that, at points where the tread intrudes the road, a counter acting contact force F builds up, proportional to the intruding distance d:

$$F = \int_0^d k(d)\, dx \tag{2.8}$$

where k is the spring stiffness. This may be a function of spring deformation but, in the standard case with a linear spring, the spring stiffness is a constant and the equation simply reduces to Hook's law.

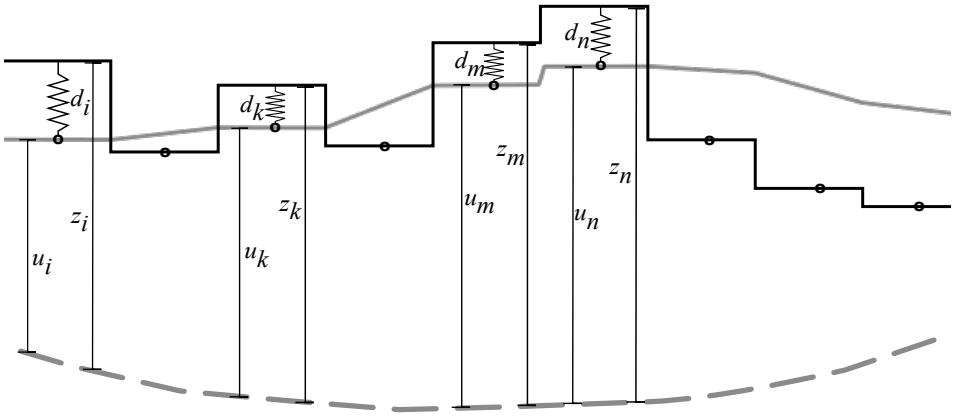

Figure 2.4: Detailed view of the contact in one time step for a few points in and out of contact. The dashed line represents the contour of the undeformed tyre, the grey line shows the contour of the deformed tyre. The height of each road element above the contour of the undeformed tyre is defined as z. Contact springs are activated at points where the tread invades the road on smaller length scales, transmitting a contact force proportional to the intruding distance d. The tyre responds to these forces (and forces acting in previous time steps) by deforming, this displacement of the tyre surface is here denoted u.

The tyre deforms due to the contact forces according to the Green's functions calculated from the WFEM. The displacement $u_{m,e}(t)$ of a point e on the tyre surface due to the contact force $F_m(t)$ at any point m in the contact patch is calculated by a convolution integral:

$$u_{m,e}(t) = F_m(t) * g_{m,e}(t) \tag{2.9}$$

where $*$ denotes the convolution operation and $g_{m,e}(t)$ denotes the displacement Green's function at element e due to a pressure impulse that is uniformly distributed over element m and that amounts to a unitary force. The total displacement response at element e, u_e, is represented by a summation of the contributions from all contact forces (at all elements):

$$u_e(t) = \sum_m u_{m,e}(t) = \sum_m F_m(t) * g_{m,e}(t) \tag{2.10}$$

The contact set-up in Figure 2.4 shows that for *every point in contact*, the displacement of the tyre, u, and the spring displacement d together equal the road height above the contour of the undeformed tyre, z. To find the share between the two

components u and d in each time step, a function f_{NR} was set up and a Newton-Raphson algorithm was used to optimise the solution:

$$f_{\mathrm{NR}} = u + d - z = 0 \tag{2.11}$$

where d gives the contact forces according to the stiffness formulation in Equation 2.8 which in turn affects the tyre displacement via Equation 2.10.

2.5.3 Radiation module

Steady state contact forces obtained from the contact module are transformed into the frequency domain and used as excitation to the tyre WFEM. The result is frequency dependent surface vibrations. The sound radiation from these is calculated with a Half-Plane Boundary Element formulation in which the tyre is placed above an acoustically rigid ground. Interested readers may consult [78] for more detailed technical information.

Kropp et al. [35] showed that a limited number of low-order modes are responsible for the sound radiation. Hence, a set of mainly low-order modes are included in the radiation calculations, and the spatial discretisation of the tyre that is used in the contact calculations is decreased in the radiation module to obtain feasible calculation times. Furthermore, to accurately model the horn effect, the tyre mesh for the radiation calculations is based on the deformed shape of the tyre due to static loading, which follows from the tyre/road interaction calculations for the zero-frequency case (see also [76]).

2.6 Motivation

The knowledge-base of research in the tyre/road noise field is immense and spans over several decades. The present work relates to a few topics that are primarily linked to the physical modelling and prediction of tyre/road noise.

We know e.g. that the tyre/road noise prediction tool at Chalmers gives good agreement between measurements and simulations, even up to the 1250 Hz band [26, 40]. As the model does not include air-pumping, the question arises as to whether air-pumping is a significant contributor to tyre/road noise? No consensus can be found in the literature as to whether, and under what circumstances, air-pumping is an important element of in situ tyre/road noise. Could the speed dependency of different types of noise generation mechanisms be used to investigate air-pumping?

On the other side, there is also a possibility that the model overestimates the high frequency noise purely generated by tyre vibrations. The contact stiffness parameter has been shown to have a great influence on the simulated tyre/road noise. The mechanisms behind this sensitivity have, however, not been thoroughly investigated in the literature. A higher degree of control could be obtained if it was understood why the contact stiffness is so significant. This knowledge could also help us to understand what level of detail is needed in the contact model. This, in turn, could clarify the consequences of reducing complexity in the contact stiffness formulation with respect to the modelled contact forces and simulated noise.

As the contact stiffness represents displacement of tread material, it will exhibit inherent mass inertia and damping characteristics. The importance of these dynamic features depends on the material properties, the spatial discretisation and the contact process itself. A discussion about the effects of tread mass and energy losses within the tread material is often lacking in many of the existing tyre/road contact models. These parameters may be of significance, especially if the model is intended to capture detailed processes in the tyre/road contact like stick-snap, stick-slip, and small-scale air-flow in the contact patch.

Chapter 3
Contact stiffness in tyre/road noise modelling

This work is based on Paper III and Paper I. Both studies include tyre/road contact simulations in which small-scale tread deformation is accounted for by contact springs. Effects of different stiffness formulations on modelled tyre/road noise is investigated in the first two chapters. Aspects of small-scale tread dynamics are evaluated in the last chapter by modelling the contact between an elastic layer and a rough road surface on a detailed level.

3.1 Contact stiffness effects in the tyre/road noise simulation tool at Applied Acoustics

The tyre/road noise simulation tool presented in Chapter 2.5 is used here to investigate the effects of changing the single-valued stiffness of the contact springs used in the contact model to account for the small-scale roughness on length scales smaller than the spatial discretisation.

3.1.1 Tyre and road input data

The simulations employ data from two road surfaces from the Kloosterzande test tracks [79]: a rough surface with surface dressing (SD) 5/8 and a stone mastic asphalt (SMA) 0/16 surface; see Figure 3.1 for their roughness amplitude spectra.

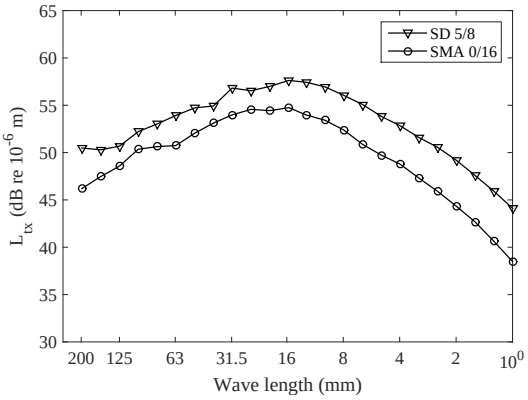

Figure 3.1: Third-octave band average of the road surface spectra for the road data used in the simulations, surface dressing (SD) 5/8 and an SMA 0/16 surface.

The rolling calculations were performed for a velocity of 90 km/h and a predetermined axle load of 2698 N. Only contact forces in the normal direction of the road are considered. The tyre waveguide finite element model is based on a Continental 205/55 R16 tyre with 20 solid elements for the tread in the lateral direction and 46 shell elements for the belt and sidewalls. The circumferential resolution is 3.8 mm. In the contact calculation, the tread elements are paired two and two, resulting in 10 elements of 2 cm width in the lateral direction. The first 25 wave orders in the circumferential direction and 20 cross-sectional modes for each wave order are considered in the radiation calculations. This has been shown to be sufficient for accurate predictions in the frequency range of interest [35]. The frequency resolution is around 6 Hz as a result of vehicle speed and spatial resolution of the contact.

The stiffness of the contact springs, k, is varied and is represented by k_α^0, where α is a spring stiffness variation factor and ^{0} indicates that the spring stiffness is a constant:

$$\mathrm{k}_\alpha^0 : \mathrm{k} = 5 \cdot 10^{3+\alpha} \quad (\mathrm{N/m}) \quad (\alpha = 0, 1, 2) \tag{3.1}$$

3.1.2 Results

The footprint of the tyre on a road due to the prescribed static load is significantly affected by the stiffness of the contact springs, as can be seen in Figures 3.2 and 3.3. Stiff springs result in fewer contact points and a concentration of the load around the highest asperities of the road. The footprint on the smoother SMA 0/16 road

has more of a dense oval shape for the softest springs compared with the SD 5/8 surface where the road roughness disrupts the symmetry.

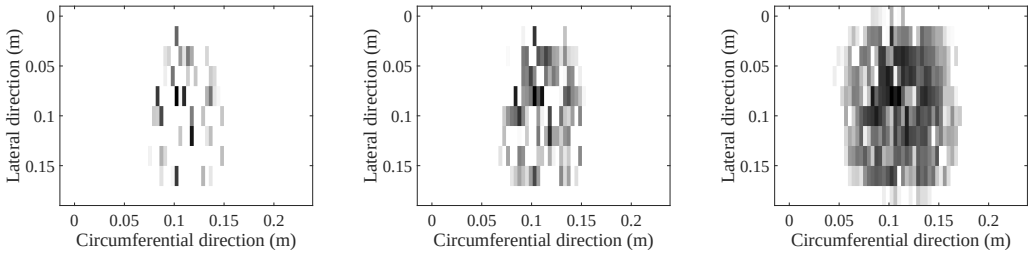

(a) $k^0_{\alpha=2}$ (b) $k^0_{\alpha=1}$ (c) $k^0_{\alpha=0}$

Figure 3.2: Footprint for a static load on the SMA 0/16 road surface using different contact stiffness.

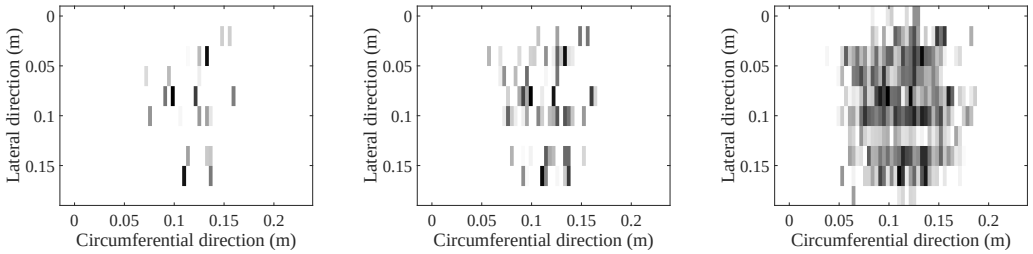

(a) $k^0_{\alpha=2}$ (b) $k^0_{\alpha=1}$ (c) $k^0_{\alpha=0}$

Figure 3.3: Footprint for a static load on the SD 5/8 road surface using different contact stiffness.

Figure 3.4 shows the simulated noise when varying the contact stiffness (not A-weighted). Stiff springs result in an greater noise. The higher frequencies are more affected, especially in the case of the SMA 0/16 road, Figure 3.4a, where the difference is as great as about 35 dB in the 1600 Hz band. The peak around 1600 Hz is suggested to be due to a contact resonance phenomenon. A similar clear increase is not seen in the case of the SD 5/8 road, Figure 3.4b, where the maximum difference of around 24 dB is found in the 1000 Hz band.

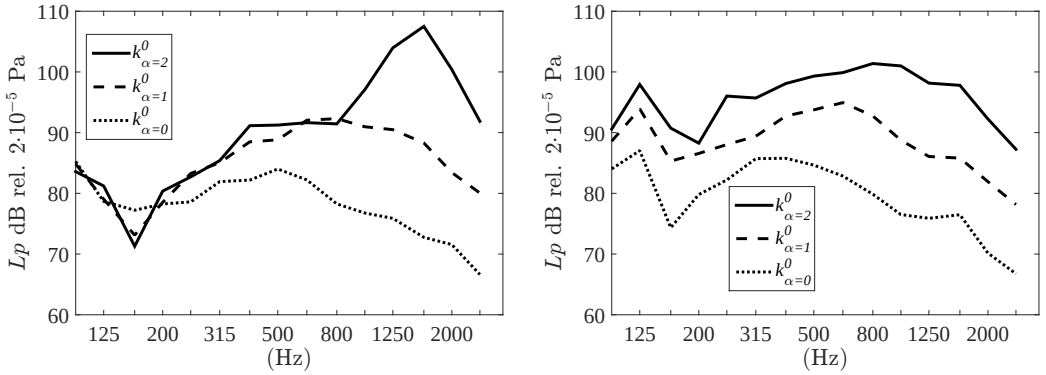

(a) SMA 0/16

(b) SD 5/8

Figure 3.4: Simulated sound pressure level for the two different roads and three values of contact spring stiffness.

Three mechanisms are suggested to be responsible for the sensitivity of the simulated tyre/road noise to changes in contact stiffness. The first is that the change in the spatial distribution of contact forces seen e.g. in Figures 3.2 and 3.3 affects the deformation of the tyre, which in turn modifies the horn effect. However, this mechanism was found to have little effect on the sound pressure level in Paper III, where is was tested by interchanging the deformed tyre shape (obtained with different contact springs) in the radiation calculations, see Section 3.4 and Figure 7 in Paper III.

The second suggested explanation as to why the simulated tyre/road noise increases with increasing contact stiffness is simply that the excitation force itself depends on the stiffness in a corresponding way. Figure 3.5 shows the spectra of the total contact force for the two roads when varying contact stiffness.

The trends in the figures are similar as to seen in the simulated sound pressure level: An increased spring stiffness results in a greater contact force level and a louder tyre/road noise. For the SMA 0/16 road, the difference increases with frequency, and the pronounced peak around the 1600 Hz band seen in the sound pressure level for is also seen in the force spectrum. The maximum difference in force level is around 33 dB. The largest difference between the cases of soft and stiff contact springs for the rougher SD 5/8 road is around 24 dB and found in the 1000 Hz band.

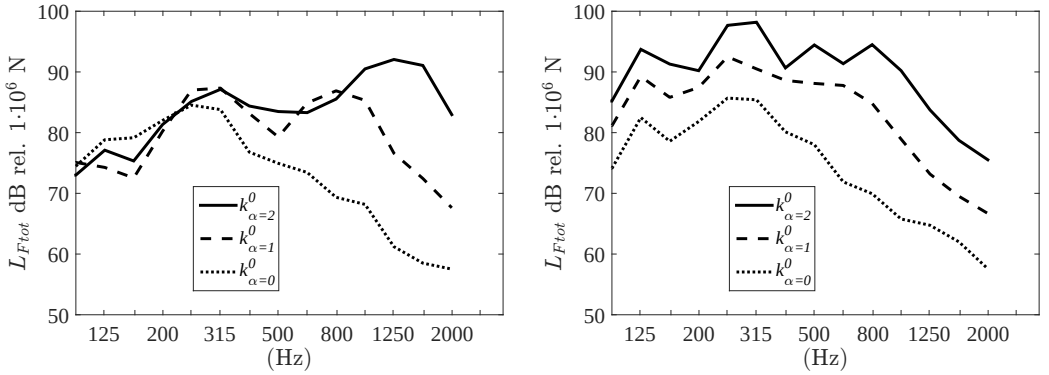

(a) SMA 0/16

(b) SD 5/8

Figure 3.5: Simulated total contact force level for the two different roads and three values of the contact spring stiffness.

A connection factor, C_F, is defined in Equation 3.2 in order to investigate the connection between the contact force level, L_F, and the sound pressure level L_p as a function of frequency:

$$C_F = 10 \cdot log_{10}\left(\frac{10^{\frac{L_p}{10}}}{10^{\frac{L_F}{10}}}\right) \tag{3.2}$$

Figure 3.6 shows the connection factors when varying the contact stiffness on the two different roads. It is seen that C_F varies between -5 dB around the 250 Hz band up to almost +20 dB for the highest third-octave bands. These tendencies are seen for both roads, but there are deviations in the middle of the frequency range. Interestingly, the different stiffness cases result in similar connection factors, which implies that the total contact force is a factor from which the radiated sound can be derived. Perhaps these results are not so surprising as correlations between measured tyre/road noise and calculated contact forces have been shown in the literature, see e.g. Dubois et al. [16].

As C_F is defined for the sum of the contact forces, the results also imply that the spatial distribution of the contact force may be neglected, at least as a first approximation, when simulating tyre/road noise. On the other hand, the connection factor shown here seems, to some degree, road specific and it has not yet been investigated how it varies with other aspects like tyre model, load and speed.

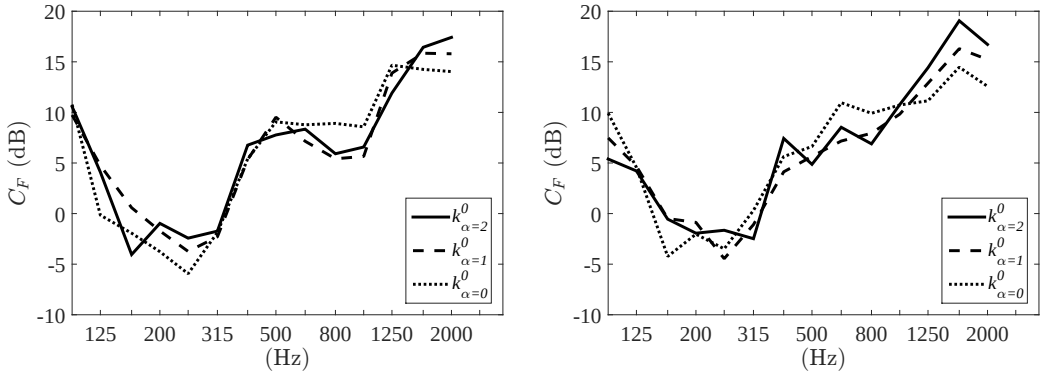

(a) SMA 0/16

(b) SD 5/8

Figure 3.6: Connection factor defined in Equation 3.2 for the two different roads and three values of the contact spring stiffness.

A third mechanism that could contribute to the sensitivity of the simulated sound pressure level to changes in the contact stiffness parameter, is the modal composition of the vibrational field of the tyre during rolling. As some modes are better sound radiators than others, the overall radiation characteristics depend on how well these are excited. And as different contact spring stiffness results in different spatial distribution of the contact forces, it is interesting to investigate whether this alters the excitation of tyre modes.

The vibrational field on the tyre is described in Equation 2.5 as a sum of the contributions from cross-sectional modes in combination with circumferential waves travelling in the positive and negative direction respectively. The total modal energy level, $L_{mod.en.}$, in a single third-octave band including angular frequencies from ω_l to ω_u, see Equation 3.3, is mapped against polar order n and cross-sectional mode number i. The present analysis focuses on frequency bands where different contact stiffness values result in large differences in radiated noise.

$$L_{mod.en.}(n,i) = 10 \cdot log_{10}\left(\sum_{\omega_l}^{\omega_u} |A_{n,i}(\omega)|^2 + |B_{n,i}(\omega)|^2 \right) \tag{3.3}$$

Figure 3.7 shows the total spectral energy level of the modal amplitudes in the 1600 Hz band on the SMA 0/16 road, where the result using very stiff contact springs (3.7a) can be compared with the case when using very soft contact springs (3.7b). Similar patterns of modal energies are seen in the two cases, but the magnitudes are significantly lower when using softer springs. The mean value of the difference in modal energy between the two stiffness cases is around 26 dB and

Figure 3.8 illustrates how it varies with different combinations of n and i. The difference varies roughly between 17–38 dB with a slight tendency for an increased contact stiffness to result in increased modal energy for combinations of low polar orders n and/or low cross-sectional mode number i.

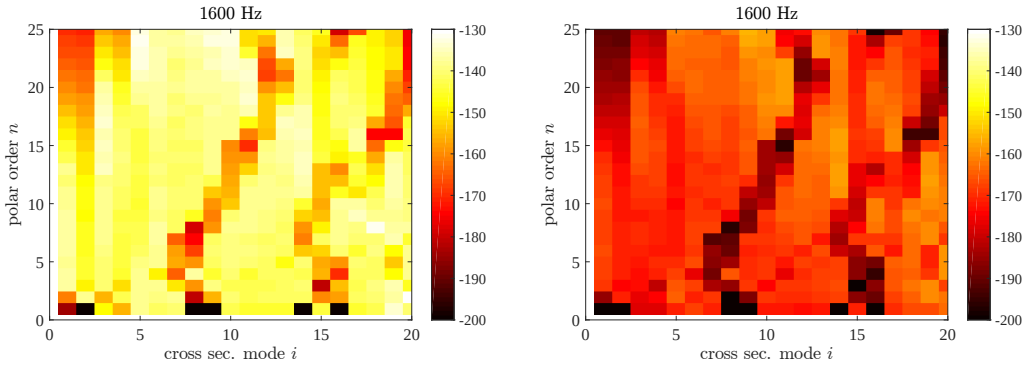

(a) $k^0_{\alpha=2}$ (b) $k^0_{\alpha=0}$

Figure 3.7: The spectral energy of the different modes in the third-octave band of 1600 Hz for the SMA 0/16 road.

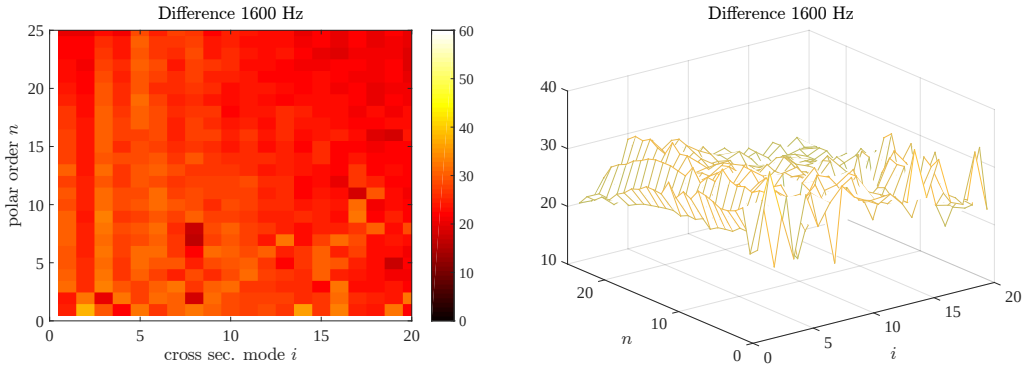

(a) $\Delta L_{mod.en.}$ (b) $\Delta L_{mod.en.}$

Figure 3.8: Difference in spectral energy between the case with stiff contact springs ($\alpha = 2$) and the case with soft contact springs ($\alpha = 0$) in the third-octave band of 1600 Hz for the SMA 0/16 road.

The corresponding results for the 1000 Hz band on the SD 5/8 road is shown in Figures 3.9 and 3.10. The mean value of the difference in modal energy between the two stiffness cases is less than for the SMA 0/16 road, around 21 dB, and it also varies less when mapped against n and i as seen in Figure 3.10.

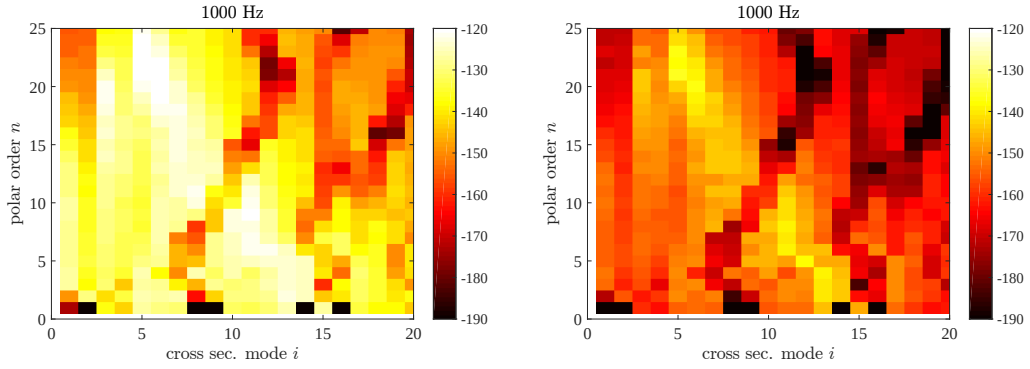

(a) $k^0_{\alpha=2}$ (b) $k^0_{\alpha=0}$

Figure 3.9: The spectral energy of the different modes in the third-octave band of 1000 Hz for the SD 5/8 road.

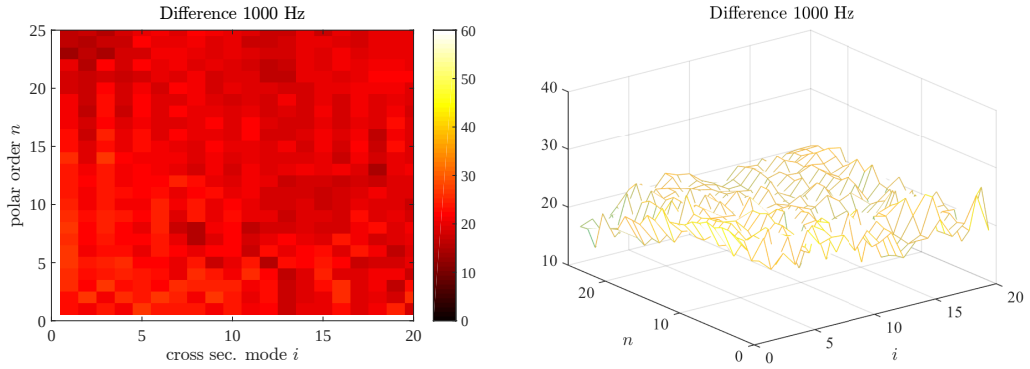

(a) $\Delta L_{mod.en.}$ (b) $\Delta L_{mod.en.}$

Figure 3.10: Difference in spectral energy between the case with stiff contact springs ($\alpha = 2$) and the case with soft contact springs ($\alpha = 0$) in the third-octave band of 1000 Hz for the SD 5/8 road.

3.1.3 Conclusions

The stiffness of the contact springs affects the simulated tyre/road noise to a great degree, an increased stiffness gives an increase in the radiated sound pressure level. Three mechanisms have been suggested: Modification of the horn effect, changes in the modal composition of the vibrational field on the tyre and increase of the contact forces exciting tyre vibrations. Results show that the variation in the total contact force is the most important reason for the sensitivity of the simulated noise to variations in contact stiffness.

A connection factor was defined that estimates the relationship between total modelled contact force and simulated sound pressure level. It can be seen as an approximative representation of the radiation module in the tyre/road noise simulation tool which was briefly covered in Chapter 2.5.3. The connection factor is surprisingly stable, the small variations that still can be seen are believed to be coupled with the small changes in modal composition that can be found for different stiffness cases.

The connections factor could perhaps be used when performing parameter studies as a first estimate to circumvent the computationally heavy radiation calculations. However, if a greater precision is sought in the simulated tyre/road noise, the modal composition of the vibrational field on the tyre should also be considered.

3.2 Contact springs with non-linear stiffness

The contact stiffness parameter has a great influence on the modelled contact forces and simulated tyre/road noise. The idea of the following investigation was to learn what difference it makes if contact springs with non-linear stiffness are used compared to the ones with constant stiffness that are presently implemented in the contact model. This as non-linear stiffness functions are suggested to better represent the gradual contact between a real tyre tread and road surface than a single stiffness value.

3.2.1 The stiffness functions

This study uses a somewhat rough approach to the stiffness function, as the purpose of the investigation is foremost to see if it is feasible to implement non-linear contact stiffness functions in the present model and if so, what effect they have on the result. Based on the understanding of the influence of using non-linear contact

springs, it may be worth investigating more elaborate methods to determine the stiffness functions to the degree needed for the simulation model.

Contact stiffness functions that grow linearly, k^1, with spring displacement d were tested as well as stiffness that grows quadratically with spring displacement, k^2:

$$k^1: \quad k(d) = 5 \cdot 10^{6+\beta} \cdot d \quad \text{(N/m)}$$

$$k^2: \quad k(d) = 5 \cdot 10^{9+\beta} \cdot d^2 \quad \text{(N/m)}$$

The β is to indicate that two *versions* of the stiffness functions were used, one softer with $\beta = 0$, and one stiffer with $\beta = 2$.

Non-linear stiffness functions that are based on the roughness of the roads were also tested. The idea was schematically introduced in Chapter 2.2 (see e.g. Figure 2.2). The height distribution of the two roads used here can be seen in Figure 3.11. The smoother SMA 0/16 surface shows a rapid increase in elements, whereas the SD 5/8 has an initial slower increase as expected for rougher surfaces. These height distribution functions are then scaled to represent stiffness as a function of spring deformation, with the maximum stiffness set to either 10^5 or 10^7 N/m at full contact. The stiffness functions based on road roughness can thus be expressed in a similar way as k^1 and k^2 with the same version factor β:

$$k^{\mathrm{SMA\,0/16}}: \quad k(d) = 10^{\beta} \cdot k^{\mathrm{SMA\,0/16}}(d) \quad \text{(N/m)}$$

$$k^{\mathrm{SD\,5/8}}: \quad k(d) = 10^{\beta} \cdot k^{\mathrm{SD\,5/8}}(d) \quad \text{(N/m)}$$

The three constant stiffness values k^0 that were presented in Chapter 3.1 are included for comparison. In the following, their results will be shown with thick grey lines with the same line type as shown earlier, e.g. in Figure 3.4.

All resulting stiffness functions are shown in Figure 3.12. Figure 3.13 shows the corresponding spring force as a function of spring deformation. For smaller spring deformations, the spring stiffness (and force) is, as expected, considerably smaller for the non-linear springs compared with the constant stiffness cases. For larger spring deformations, the non-linear functions grow past the constant values. Where this crossing appears, depends on the function and the stiffness version factor α and β.

One can argue that the stiffness functions are extreme and hence the results are extreme. There is no claim to have found representative/suitable stiffness functions, instead the aim is foremost to test different alternatives.

A few words concerning the present implementation of the road-specific functions and how they act in the contact calculations may be useful. The work is currently done in Matlab, where the stiffness functions are constructed from a piecewise

linear interpolation of the specific height distribution functions in Figure 3.11, scaled to a maximum stiffness, and eventually resulting in a `cfit` object. This object returns the corresponding stiffness of any value of spring deformation. When the spring force is required, the `integrate` function is called with the `cfit`-object and the spring deformation value. The computational effort of the contact calculations was expected to increase with this procedure compared to cases with analytical stiffness functions. However, the increase was actually found to be minor.

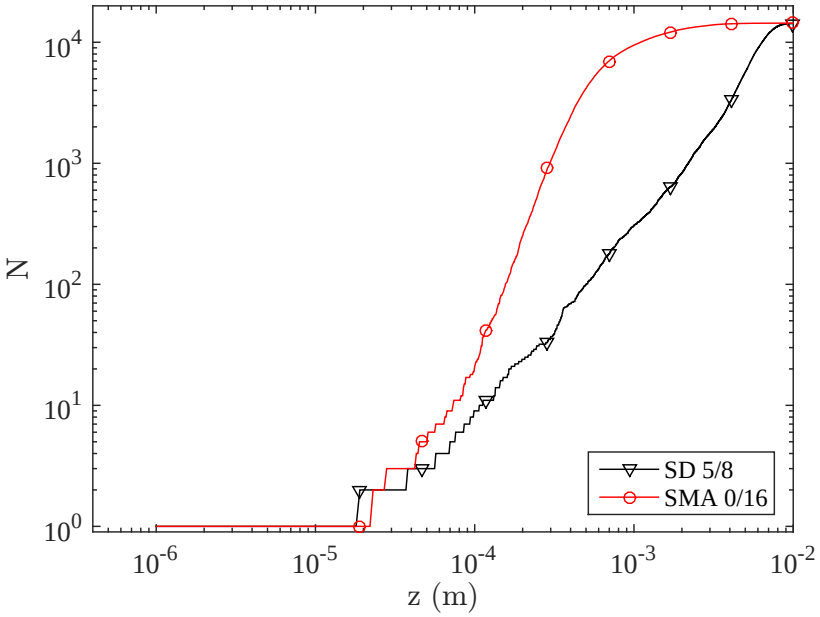

Figure 3.11: Height distribution showing the number of road elements above the height z for one track on the two roads included in the simulations. The vertical increment here is $1 \cdot 10^{-6}$ m. The idea was presented in Chapter 2.2, see Figure 2.2.

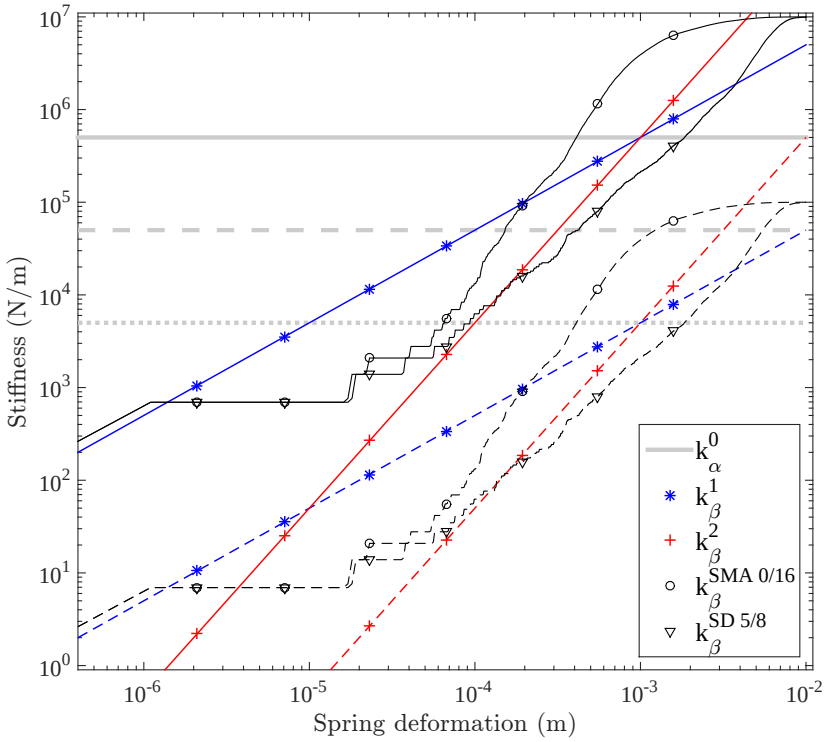

Figure 3.12: Contact stiffness as a function of spring deformation for different stiffness functions. Constant stiffness k^0 ($\alpha = 0$, 1, 2), the analytical non-linear functions: k^1, k^2 ($\beta = 0$, 2). And stiffness functions based on the height distribution of the road: $k^{\text{SMA 0/16}}$ and $k^{\text{SD 5/8}}$. The dashed lines represent the softer versions of the non-linear functions, i.e. $\beta = 0$.

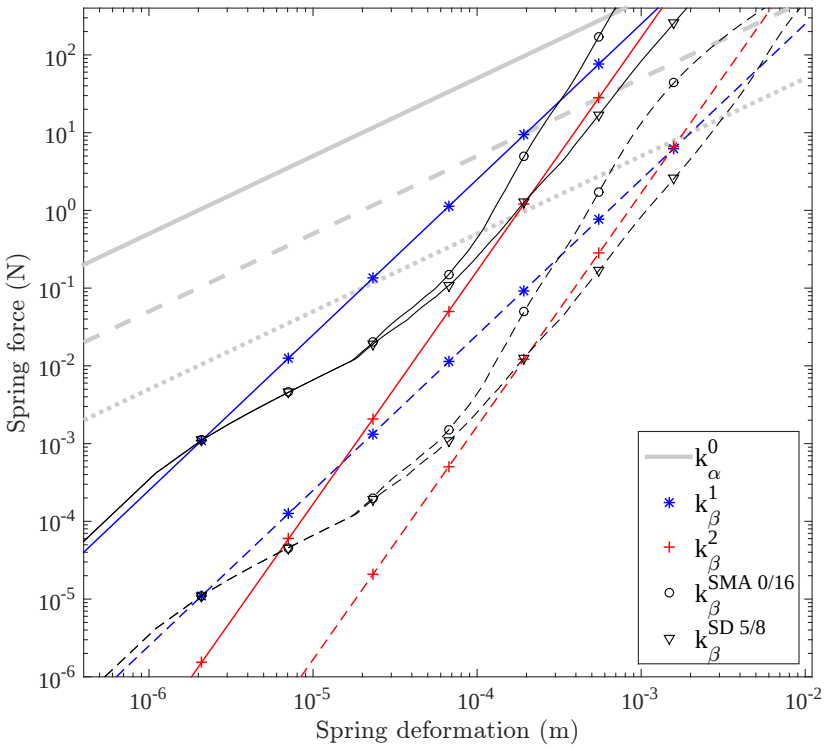

Figure 3.13: Contact force as a function of spring deformation for different stiffness functions. Constant stiffness k^0 ($\alpha = 0$, 1, 2), the analytical non-linear functions: k^1, k^2 ($\beta = 0$, 2). And stiffness functions based on the height distribution of the road: $k^{\text{SMA } 0/16}$ and $k^{\text{SD } 5/8}$. The dashed lines represent the softer versions of the non-linear functions, i.e. $\beta = 0$.

3.2.2 Simulation results

Figure 3.14 shows the resulting simulated sound pressure level using the different contact stiffness functions on the two different roads. Figure 3.15 shows the corresponding total contact force level and Figure 3.16 the connection factor as defined in Equation 3.2.

The simulated sound pressure level using non-linear contact stiffness functions is in the same range as cases with constant contact stiffness. The tendencies are also similar with e.g. less contact stiffness sensitivity of the results in the low-mid frequency range for the SMA 0/16 road (Figure 3.14a and 3.15a).

The softer non-linear cases ($\beta = 0$), however, give significantly less high-frequency noise than the softest constant-stiffness spring ($\alpha = 0$). This results in differences in the sound pressure level of up to 50 dB between different contact stiffness cases.

The most distinctive difference between results using a single-valued or a non-linear stiffness is that the latter results in a sound pressure level that drops off more at higher frequencies. This is also seen in the total contact force results. Compare e.g. the single-valued stiffness case with $\alpha = 1$ with the $k_{\beta=0}^{\mathrm{SMA\ 0/16}}$ case in Figure 3.14a. They follow each other closely up to the 800 Hz band, but then the non-linear case decreases about 30 dB to the 2000 Hz band whereas the constant stiffness case only drops a little bit more than 10 dB.

The stiffest non-linear cases with $\beta = 2$ on the SMA 0/16 road also capture the pronounced noise peak around the 1250-1600 Hz bands that was also seen in the case with the stiffest constant value. An increase is also seen in the contact force results of the stiffest cases, indicating influence from a contact resonance phenomenon. As the connection factor is high around these frequency bands, the sound pressure level has an even more pronounced peak than the contact force spectrum.

Using non-linear contact stiffness functions does not alter the connection factor between force and noise as seen in Figure 3.16. It varies up to 5 dB between different stiffness functions in some frequency bands.

The implementation of analytical non-linear stiffness functions, k^1 and k^2, is an extension to what is included in Paper III. The similarity in the results compared when using the numerical versions of road specific functions, indicates that the contact model works as expected.

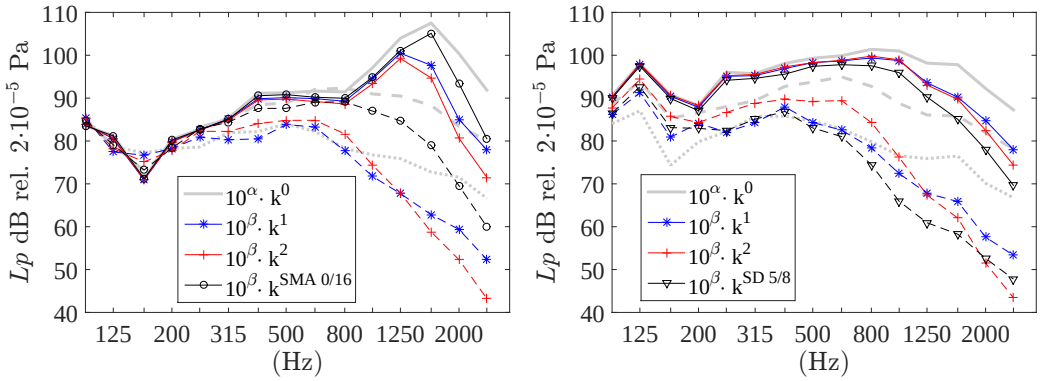

(a) SMA 0/16 (b) SD 5/8

Figure 3.14: Simulated sound pressure level for the different stiffness functions on the two roads. Constant stiffness k^0 with $\alpha = 0$, 1, 2. Non-linear functions: k^1, k^2 with $\beta = 0$, 2. Road-specific stiffness functions: (a) $k^{\text{SMA 0/16}}$ and (b) $k^{\text{SD 5/8}}$. Dashed lines represent the softer versions of the non-linear functions, i.e. $\beta = 0$.

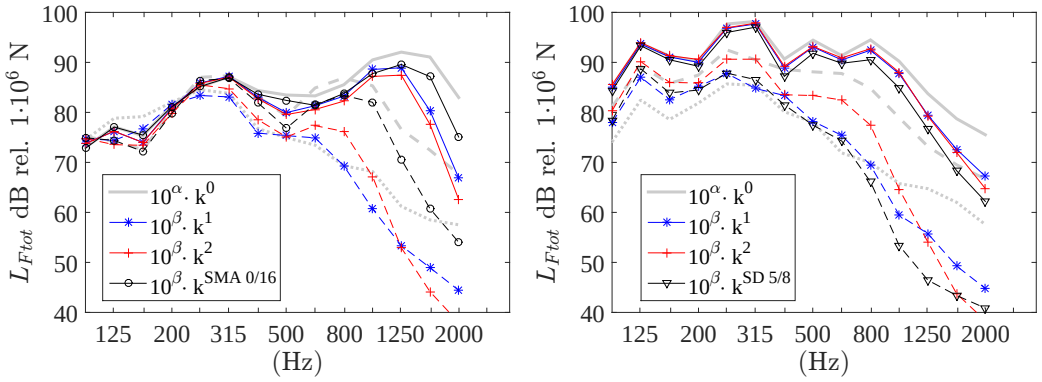

(a) SMA 0/16 (b) SD 5/8

Figure 3.15: Simulated total contact force level for the different stiffness functions on the two roads. Constant stiffness k^0 with $\alpha = 0$, 1, 2. Non-linear functions: k^1, k^2 with $\beta = 0$, 2. Road specific stiffness functions: (a) $k^{\text{SMA 0/16}}$ and (b) $k^{\text{SD 5/8}}$. Dashed lines represent the softer versions of the non-linear functions, i.e. $\beta = 0$.

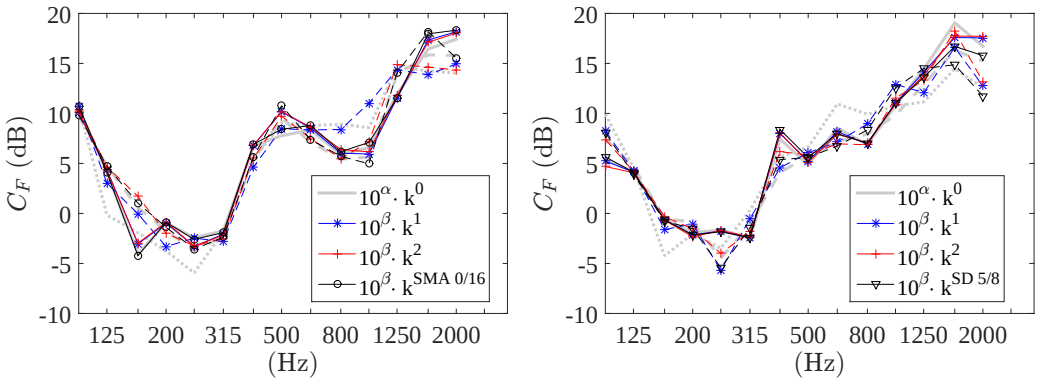

(a) SMA 0/16 (b) SD 5/8

Figure 3.16: Connection factor defined in Equation 3.2 for the different stiffness functions on the two roads. Constant stiffness k^0 with $\alpha = 0, 1, 2$. Non-linear functions: k^1, k^2 with $\beta = 0, 2$. Road specific stiffness functions: (a) $k^{\text{SMA } 0/16}$ and (b) $k^{\text{SD } 5/8}$. Dashed lines represent the softer versions of the non-linear functions, i.e. $\beta = 0$.

Detailed contact parameters

It can be suspected that the frequency behaviour of the simulation results for cases with different non-linear contact stiffness depend on the active working point of the spring deformation. In practice this corresponds to where on the x-axis in Figure 3.12 the contact develops and what maximum deformation is reached for the different cases. To investigate this, detailed contact point parameters are examined more closely in the following. Spring deformation d, active spring stiffness, k, and contact force, F, are plotted for a single contact point as a function of time. The average spectra of these parameters over several hundred contact points are also presented. Due to the limited number of time samples, the frequency resolution is just above 100 Hz.

Figure 3.17 shows an example of how the contact develops over time at a single point on the SMA 0/16 road for the different stiffness cases. A corresponding result for the rougher SD 5/8 road is seen in Figure 3.19. The specific contact points are chosen as they are representative of the specific road under study. It should, however, be noted that there is a large variation in contact development between different points in terms of duration, strength and even ranking of the different stiffness cases.

Softer springs generally result in larger spring deformation and longer contact durations. In the cases with constant-stiffness springs, only two stiffness values are possible, either maximum stiffness when in contact or zero when not in contact. The cases with non-linear stiffness functions have a less abrupt progression. The contact force develops over time as described by the spring deformation together with the stiffness function. Consequently, the cases with non-linear stiffness functions have smoother development of the contact force than the linear cases. The smoother the contact force changes over time, the faster the spectrum will decay at higher frequencies.

The average spectra of the spring deformation, contact stiffness and contact force for the different stiffness cases on the SMA 0/16 road are shown in Figure 3.18 and for the SD 5/8 road in Figure 3.20.

The results at higher frequencies seem connected with low contact forces and small deformations of the springs, which means that the working point at high frequencies is in the soft stiffness region for the non-linear springs. When studying the time signals in Figures 3.17 and 3.19, it is seen that the high-frequency content is primarily found at the onset and end of the contact, so high frequencies are necessary to go from “no contact” to “contact” and “full contact”.

A certain high-frequency component while in full contact can sometimes be seen for the very stiffest cases. See e.g. the spring displacement d and the contact force F in Figure 3.17, where a small waviness in the time signals can be observed. The frequency of this contact resonance is estimated to be around 1500 Hz, which actually matches a small increase in the spring compression and force spectrum in Figure 3.18. This is also in agreement with the pronounced hump in the spectrum of the sound pressure level and the total contact force level, Figure 3.14a and 3.15a, already assumed to be related to a contact resonance phenomenon. A similar concentrated contact resonance is not so clearly seen for the case of the rough road with surface dressing 5/8, Figures 3.19 and 3.20. This could be due to the large variation in road element heights, which randomises the contact so that the resonance is masked by the roughness excitation in the frequency range below 1000 Hz.

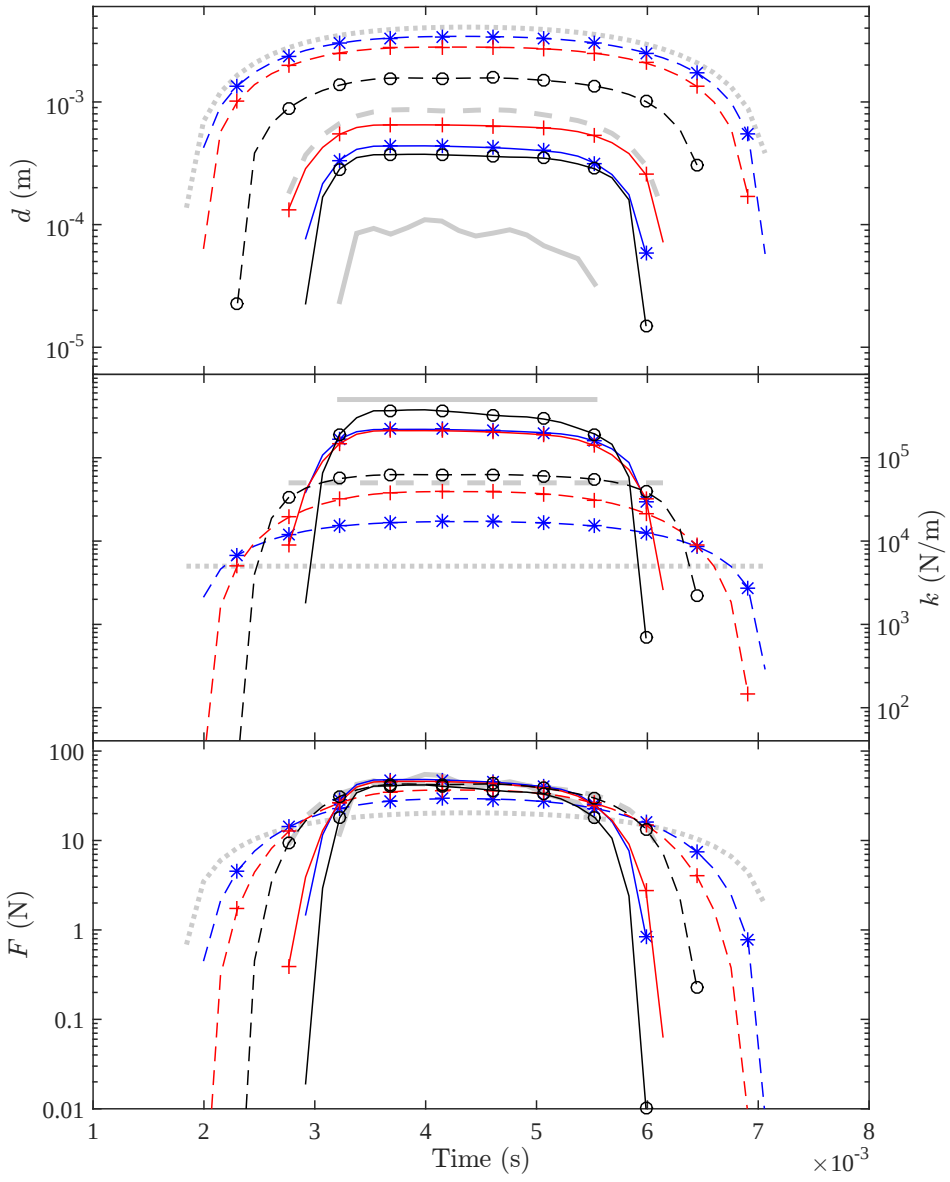

Figure 3.17: Example of the time development for a single contact point on the SMA 0/16 road. Constant springs $k^0_{\alpha=2}$(-), $k^0_{\alpha=1}$(--), $k^0_{\alpha=0}$(···) and non-linear springs $k^1_{\beta=2}$(-∗), $k^1_{\beta=0}$(--∗), $k^2_{\beta=2}$(-+), $k^2_{\beta=0}$(--+) and $k^{\text{SMA 0/16}}_{\beta=2}$(-○) and $k^{\text{SMA 0/16}}_{\beta=0}$(--○).

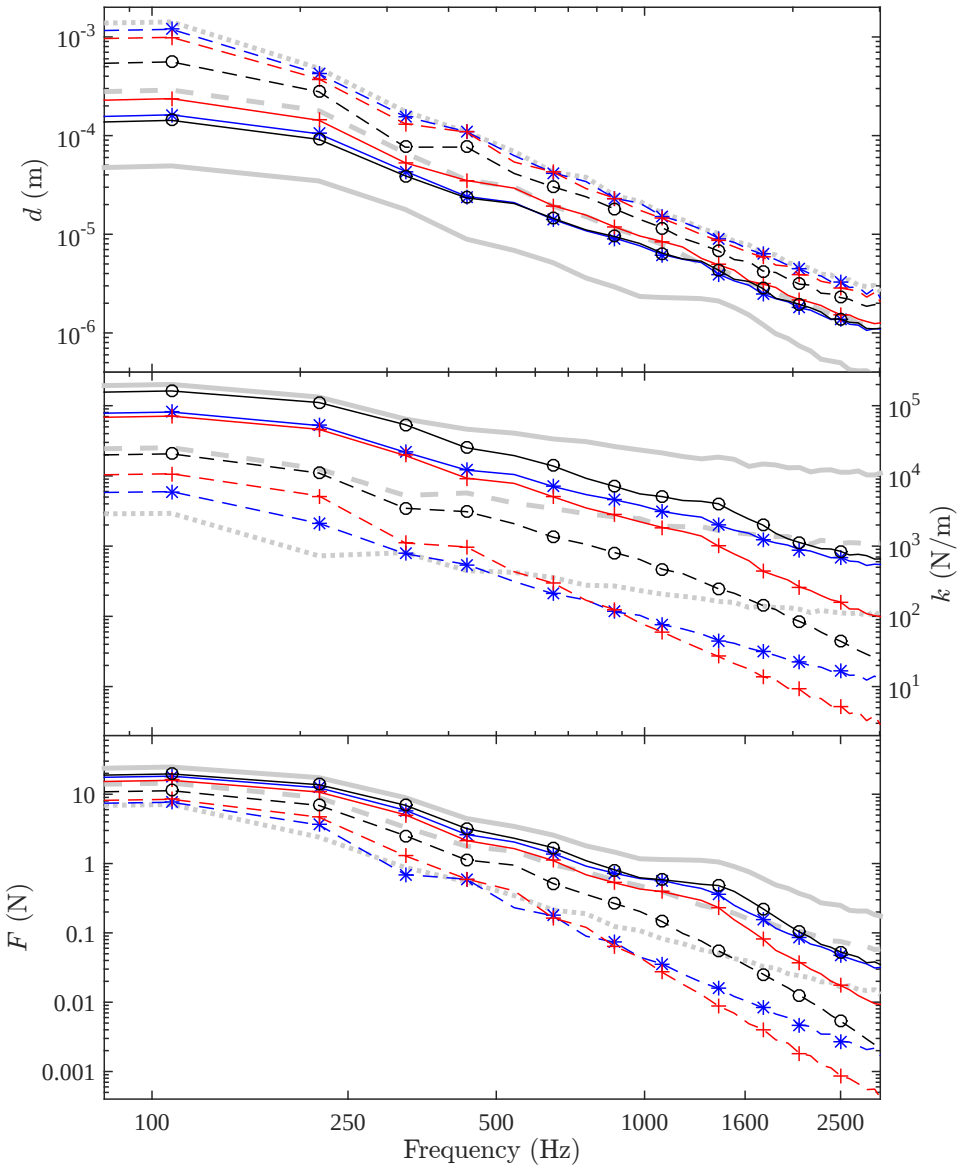

Figure 3.18: Average spectra of spring parameters for the SMA 0/16 road. Constant springs $k^0_{\alpha=2}$(-), $k^0_{\alpha=1}$(--), $k^0_{\alpha=0}$(···) and non-linear springs $k^1_{\beta=2}$(-∗), $k^1_{\beta=0}$(--∗), $k^2_{\beta=2}$(-+), $k^2_{\beta=0}$(--+) and $k^{\text{SMA 0/16}}_{\beta=2}$(-○) and $k^{\text{SMA 0/16}}_{\beta=0}$(--○).

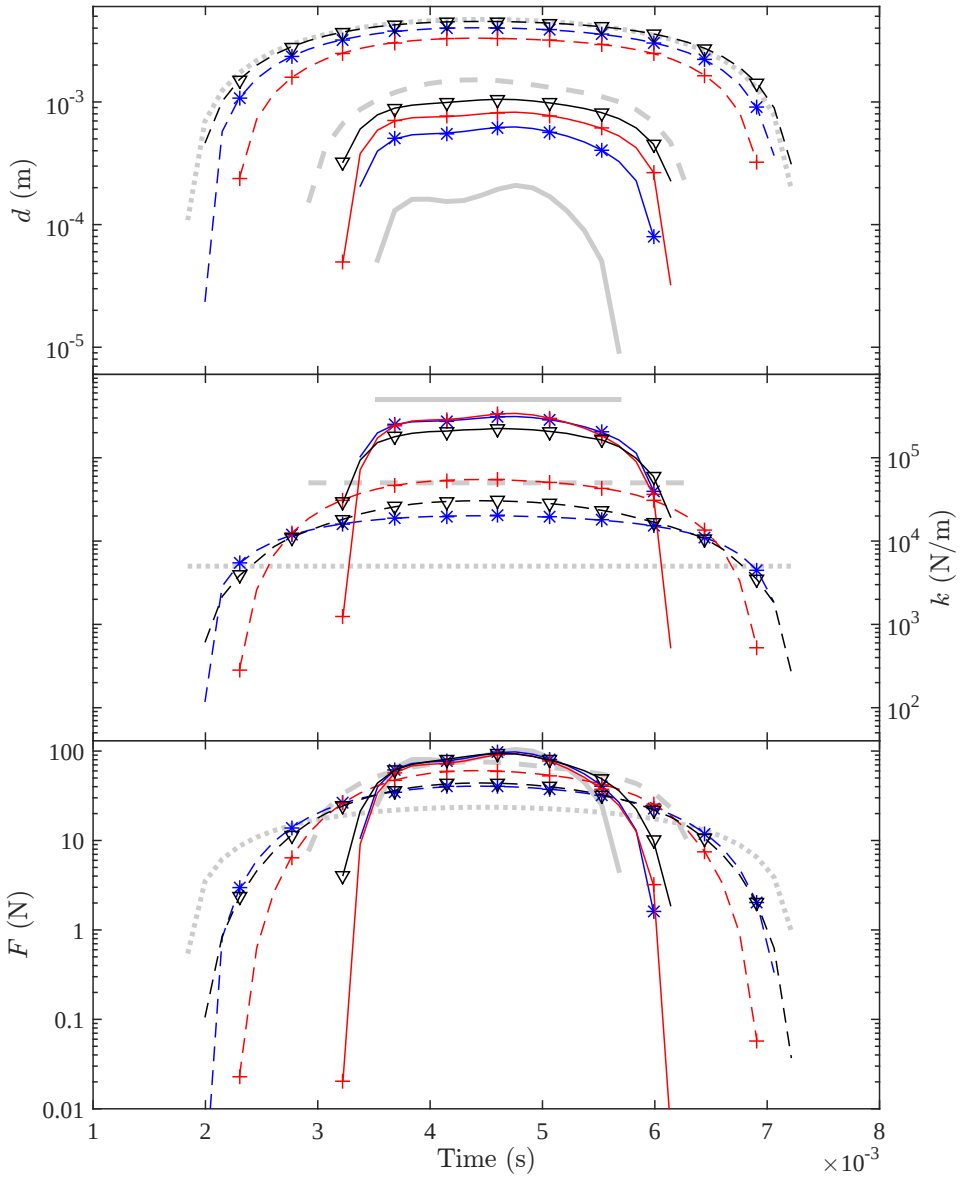

Figure 3.19: Example of the time development for a single contact point on the SD 5/8 road. Constant springs $k^0_{\alpha=2}$(-), $k^0_{\alpha=1}$(--), $k^0_{\alpha=0}$(···) and non-linear springs $k^1_{\beta=2}$(-∗), $k^1_{\beta=0}$(--∗), $k^2_{\beta=2}$(-+), $k^2_{\beta=0}$(--+) and $k^{\text{SD }5/8}_{\beta=2}$(-▽) and $k^{\text{SD }5/8}_{\beta=0}$(--▽).

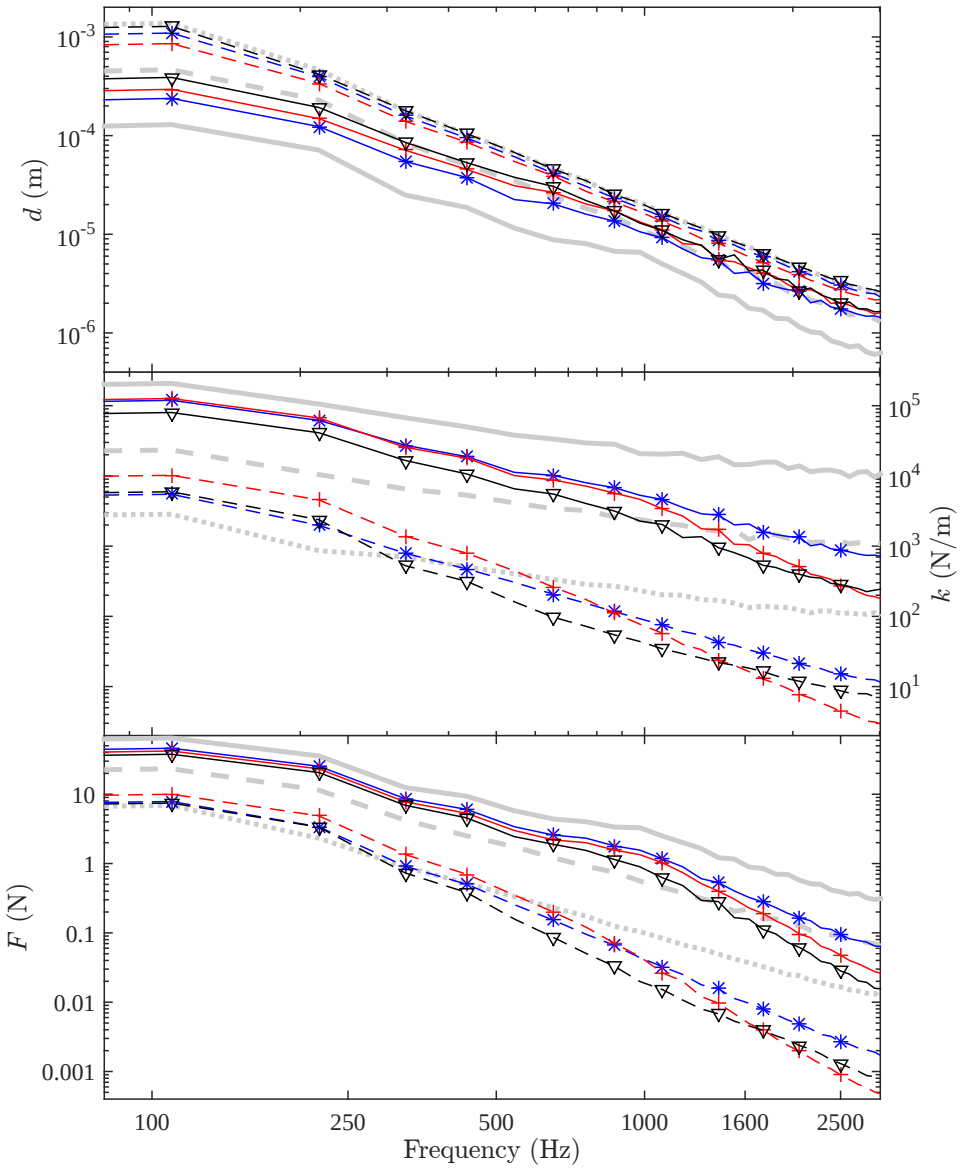

Figure 3.20: Average spectra of spring parameters for the SD 5/8 road. Constant springs $k^0_{\alpha=2}$(-), $k^0_{\alpha=1}$(--), $k^0_{\alpha=0}$(···) and non-linear springs $k^1_{\beta=2}$(-∗), $k^1_{\beta=0}$(--∗), $k^2_{\beta=2}$(-+), $k^2_{\beta=0}$(--+) and $k^{\mathrm{SD}\,5/8}_{\beta=2}$(-▽) and $k^{\mathrm{SD}\,5/8}_{\beta=0}$(--▽).

An interesting extension to the present work could be to implement damping in the contact spring formulation. Hoever included a non-linear damping feature to the constant stiffness contact springs in [45]. It is expected that damping in the contact formulation will reduce the influence of contact resonance phenomena.

3.2.3 Conclusions

Non-linear contact stiffness functions, with a stiffness that grows with spring compression, have successfully been implemented in the contact model. Both analytical functions and numerical based on road specific roughness hight distribution, are tested. The results show a reduced content of high frequencies in the contact force and the generated noise, compared with cases with a constant value of the spring stiffness.

The time evolution of the contact process at individual contact points reveal that softer springs generally results in larger spring deformation and longer contact durations. The cases with non-linear stiffness functions have a more gradual development of the contact force than the cases with constant spring stiffness. The smoother the contact force changes over time, the faster will the spectrum decay at higher frequencies.

Results at higher frequencies can be linked with low contact forces and small spring deformations, which means that the working point at high frequencies is in the soft stiffness region for the non-linear springs. Some high frequency component while in full contact, i.e. larger spring deformations, can, however, sometimes be seen for the very stiffest cases on the smoother SMA 0/16 road surface. This is suggested to be connected with the contact resonance phenomenon that distinguish itself when using very stiff springs, both linear and non-linear.

3.3 Highly detailed contact model

This chapter is based on Paper I and the licentiate thesis [80]. The goal is to investigate the effect of including/excluding damping and inertia of the tread when modelling very detailed tyre/road contact.

3.3.1 Simulations with a detailed contact model

The detailed contact model used here is based on the work of Andersson and Kropp [48] and is formulated in the time domain. Contact force and effective contact stiffness are studied as a tread layer makes contact with a 2x2 cm^2 road surface block. The two bodies are discretised into 400 (matching) elements, and the softening effect of the small-scale roughness within each element is accounted for by non-linear contact springs, schematically illustrated in Figure 3.21. The spring stiffness functions are obtained by a model of a flat circular punch indenting an elastic layer [81] according to the unique height distribution of the roughness within each element and the elastic modulus of the tread material.

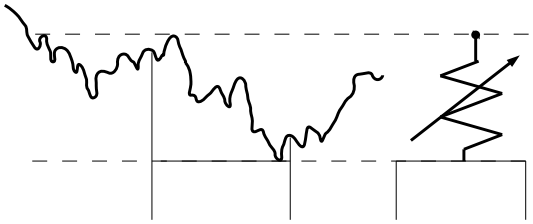

Figure 3.21: The softening effect of the road roughness within one road element is approximated by a non-linear contact spring with a unique stiffness function according to the small-scale height distribution.

The tread layer is modelled with a modified version of the two-layered elastic plate model presented and validated in [82, 24]. The resulting frequency response functions are transformed into time-domain Green's functions using an inverse Fourier transform technique. Input data representing a 1.0 cm thick elastic layer with a perfectly rigid backing are used here. Density and loss factor of the elastic layer are varied in the dynamical calculations, which are compared with the case of a quasi-static contact.

Two contact scenarios are used, the "infinite belt impedance"-case where the tread layer is forced vertically into the road surface according to a predetermined indentation acceleration as a function of time (50 m/s^2, 250 m/s^2 and 500 m/s^2). The

second case describes the contact when the elastic layer is assigned an effective mass of 5 grams and released from different heights (0.1, 0.3 and 0.4 meter) above the road patch. The released mass scenario represents an extreme case with very low impedance behind the tread layer. A predetermined indentation function represents another extreme case with an infinite belt impedance. The results of the two scenarios approach each other if the mass of the falling body is increased.

3.3.2 Results

Figure 3.22 shows the total contact force in the normal direction and contact stiffness as function of indentation for the infinite belt impedance cases. Contact stiffness is defined as the derivative of the total contact force with respect to indentation. The dynamic contact force at a given indentation of the elastic layer depends strongly on the predetermined indentation acceleration; dynamic simulations consistently result in higher initial contact stiffness than quasi-static simulations.

Figure 3.23 shows the results when varying the loss factor of the elastic layer (Figure 3.23a) and the density of the material (Figure 3.23b). A predetermined indentation acceleration of 500 $\mathrm{m\,s^{-2}}$ is used. Increasing the loss factor gives a slightly stiffer dynamic contact and vice versa, though the character of the stiffness curve is preserved. Varying the density by a factor two affects the development of the contact slightly, but the steady state contact stiffness converges towards the same value. The quasi-static results are unaffected by the indentation acceleration and variations of elastic-layer loss factor or density as the magnitude of the material stiffness is kept constant.

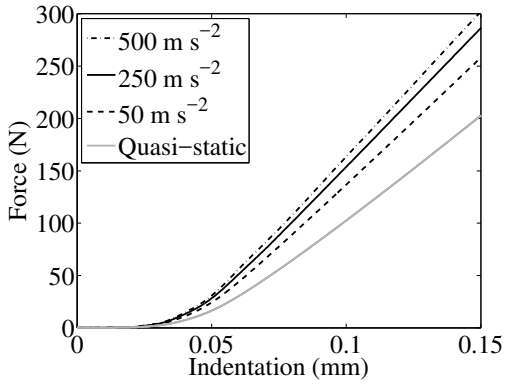

(a) Contact force as a function of indentation for different predetermined indentation accelerations and the quasi-static case.

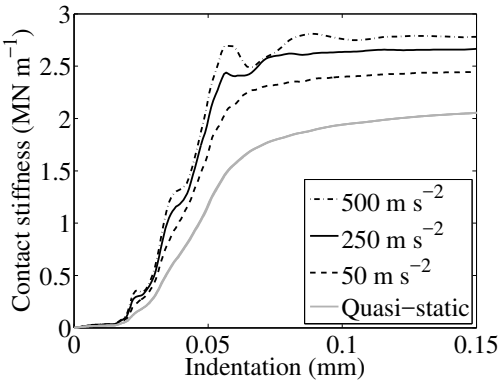

(b) Contact stiffness as a function of indentation for different predetermined indentation accelerations and the quasi-static case.

Figure 3.22: Results for different predetermined indentation accelerations and the quasi-static case.

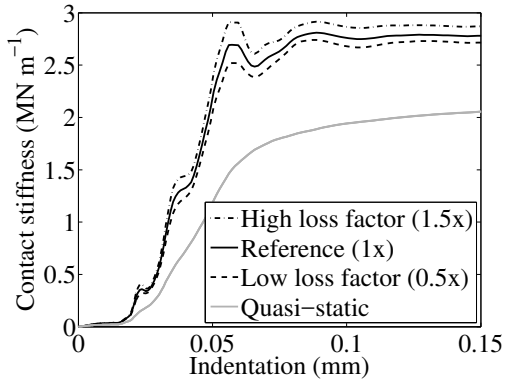

(a) Contact force as a function of indentation when varying the loss factor of the elastic layer.

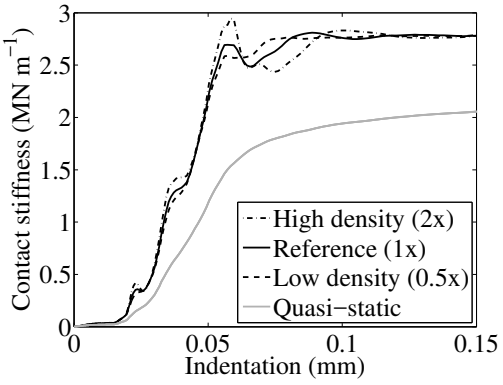

(b) Contact stiffness as a function of indentation when varying the density of the elastic layer.

Figure 3.23: Results when varying the material paramters of the elastic layer. A predetermined indentation acceleration of 500 m/s^2 is used.

The case with a small belt impedance, here modelled by a 5 gram mass dropped from different heights, is shown in Figure 3.24. The results are shown for the first contact period. The most prominent difference between dynamic and quasi-static simulations is the asymmetry introduced by the hysteresis, which is only captured when using a dynamic response of the material.

Zhang [20] found an asymmetry in the development of the measured contact force when a tyre rolls over a single asperity and noted that viscoelasticity was needed in the numerical model to simulate this behaviour. However, it is difficult to make a direct comparison between the study presented here and Zhang's work due to differences in the set-ups. The latter investigates e.g. forces during rolling, whereas the situation here is simplified to a pure vertical motion. Another apparent difference is the contact geometry; here a real road surface patch was investigated, not a single or a group of idealised asperities.

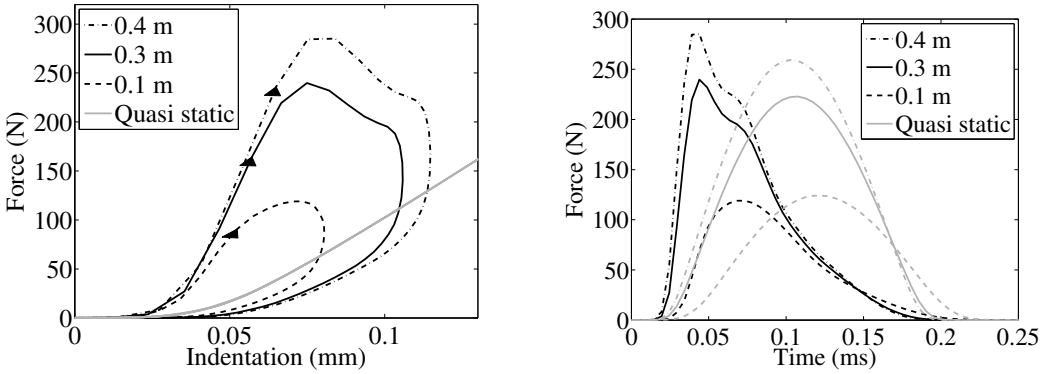

(a) Contact force as a function of indentation.

(b) Contact force as a function of time.

Figure 3.24: Dynamic and quasi-static simulations of the contact between the elastic layer and a 5 gram mass falling from three different heights.

3.3.3 Conclusions from the detailed tread/road contact model

This study investigated common approximations of the tread when modelling contact forces in tyre/road contact models on a detailed level. This was done by comparing dynamic calculations that include effects of mass and damping in the tread material with results when using a quasi-static approximation.

The stiffness function representing how the contact force changes with indentation depends on a combination of road topography, material parameters of the tread and the time development of the contact. Contact stiffness increases with

increasing predetermined indentation acceleration when using a dynamic response of the elastic layer. In the case of a quasi-static response, contact stiffness is significantly softer and impervious to the indentation acceleration. Damping in the elastic layer results in stiffer contact compared with the quasi-static case. The effect is significant, but it does not alter the character of the stiffness function. The material density does not produce any significant effects on the contact stiffness after saturation. Its major effect is small ripples on the stiffness function during the initial indentation.

It has been shown here and in the literature that a quasi-static approximation of the tread is unable to capture the dynamic development of detailed tyre/road contact. However, if modifying the stiffness, quasi-static responses can be tuned to reproduce overall contact quantities well, such as maximum contact force and contact stiffness.

3.4 Conclusions

Chapter 3 has investigated aspects of contact stiffness in the context of tyre/road noise modelling.

The stiffness of contact springs affects the simulated tyre/road noise to a large degree, an increased stiffness gives an increase in the radiated sound pressure level. Three mechanisms are thought to contribute to this sensitivity: The horn effect, the modal composition of the vibrational field of the tyre and the contact forces that excites tyre vibrations. A numerical tyre/road noise simulation tool based on physical relations is used to investigate these aspects. Results show that the variation of the total contact force is the most important factor, increased contact stiffness gives increased total contact force level.

A connection factor is defined that estimates the relationship between total modelled contact force and the simulated sound pressure level. It could e.g. be used when performing parameter studies as a first approximation to circumvent the, computationally heavy, radiation calculations. If a higher precision is sought in the simulated tyre/road noise, the modal composition of the vibrational field on the tyre should also be considered.

The contact model in the tyre/road simulation tool was extended to include non-linear contact springs with stiffness that grows with spring deformation. The results show a reduced content of high frequencies in the contact force and the generated noise, compared with cases with a constant value of the spring stiffness. The time evolution of the contact process at individual contact points revealed that cases with

non-linear stiffness functions have a more gradual development of the contact force than the cases with constant spring stiffness. The smoother a parameter changes over time, the faster will its spectrum decay at higher frequencies.

Contact resonance phenomena could be distinguished when using very stiff springs, both constant and non-linear, for the smoother of the tested road surfaces. These resulted in a significant increase in the simulated sound pressure level around the 1600 Hz band.

Effects of tread mass and damping have been studied by simulating the detailed contact between an elastic layer and a rough road surface using a previously developed numerical time domain contact model. Road roughness on length scales smaller than the discretisation scale was included by individual, non-linear contact springs between each pair of contact elements. The dynamic case, with an elastic layer impulse response extending in time, is compared with the case where the corresponding quasi-static response is used.

Results show that the resulting contact stiffness increases with increasing predetermined indentation acceleration when using a dynamic response of the elastic layer. The contact stiffness is significantly softer, and impervious to the indentation acceleration, for the case of a quasi-static response. A dynamic response of the tread also captures an asymmetry in the time development of the contact force for the simulations case with a very small belt impedance. Damping in the elastic layer gives a stiffer contact compared with the quasi-static case. The effect is significant but it does not alter the character of the contact. The material density does not produce any significant effects on the contact stiffness after saturation. Its major effect is small ripples on the stiffness function during the initial indentation.

Chapter 4

The speed exponent approach to air-pumping

This chapter is based on Paper II and the work with finding a way to distinguish the contribution from air-pumping in a set of tyre/road noise data. Some additional effort is spent on the effect of tread pattern pitch on the speed dependency of the generated noise.

4.1 The method

The idea of individual speed exponents for different noise-generating mechanisms found in the literature (e.g. [7]) has been concretised in this study into a suggested curve-fitting model. The study investigated whether tyre/road noise mechanisms can be seen as separable source terms, with different speed dependencies, together forming the sound pressure level. The sources are, as a first approximation, assumed to be uncorrelated to make the analysis feasible.

The acoustic pressure of the tyre/road noise as a function of vehicle velocity U and third-octave band centre frequency f_n ($n = 125, ..., 5000$ Hz) is modelled as:

$$p^2(f_n, U) = A_2(f_n, U) \cdot U^2 + A_4(f_n, U) \cdot U^4 + A_6(f_n, U) \cdot U^6 \tag{4.1}$$

The first term in Equation 4.1 relates to the contribution from tyre vibrations with A_2 being a coefficient determining the strength of this type of noise source. The second term, with the coefficient A_4 represents the noise from monopole-type sources, which all grow by U^4. The last term considers noise generated from wind flow around the vehicle, growing by U^6. The source coefficient A_6 is determined separately with data from wind tunnel measurements.

The next step is to assume that the source coefficients of the different types of noise sources do not depend on driving speed. This can be understood as a presumption

that there is no pitch-related phenomenon, or that there is an even or randomised distribution of pitch. This allows us to simplify our previous expression:

$$p^2(f_n, U) = A_2(f_n) \cdot U^2 + A_4(f_n) \cdot U^4 + A_6(f_n) \cdot U^6 \tag{4.2}$$

The $A_6(f_n)$ coefficients are determined from wind tunnel measurements assuming a U^6 wind speed dependency of the noise. With $A_6(f_n)$ fixed, the optimal values of $A_2(f_n)$ and $A_4(f_n)$ were sought using a curve-fitting algorithm to *model* a sound pressure level with the logarithmic form of Equation 4.2 that best fits the measured tyre/road noise sound pressure level for each frequency band.

The analysis results can be presented as ratios, R_m, representing the contribution of one source term A_m ($m = 2, 4,$ or 6) to the total source strength, see Equation 4.3. R_m is illustrated in a grey scale colour plot where brightness is proportional to the percentage of a specific source as a function of third-octave band and evaluated speed U.

$$R_m(f_n, U) = \frac{A_m(f_n) \cdot U^m}{A_2(f_n) \cdot U^2 + A_4(f_n) \cdot U^4 + A_6(f_n) \cdot U^6} \tag{4.3}$$

4.2 Data

4.2.1 Measurement data

The measurement data that are analysed in this work originates from the Sperenberg project [7], which was conducted at a former airfield in Sperenberg close to Berlin in Germany. It was a major measurement project in which thousands of controlled coast-by sound pressure levels were recorded at nominal driving speeds in the range from 50 km/h to 120 km/h. Sixteen different car tyres were tested on over 40 different road surfaces [83]. The present work applies the speed exponent approach on measured third-octave band spectra produced at the different vehicle speeds. The spectrum is based on a short segment of the coast-by noise taken when the A-weighted overall sound pressure level peaked. This introduces some uncertainty, as it is not defined where the vehicle was actually positioned when the time signal was recorded.

Wind tunnel measurements were performed as a part of the Sperenberg project with the two vehicles used in the coast-by measurements, a Volkswagen Polo and a Mercedes C-type. The report [7] presents third-octave band results for the latter vehicle at three wind speeds, 80, 100 and 120 km/h, see Figure 4.1. For the present

work, these results were extracted and a U^6 curve was fitted to them, resulting in an estimate of the contribution from wind noise in the coast-by measurements.

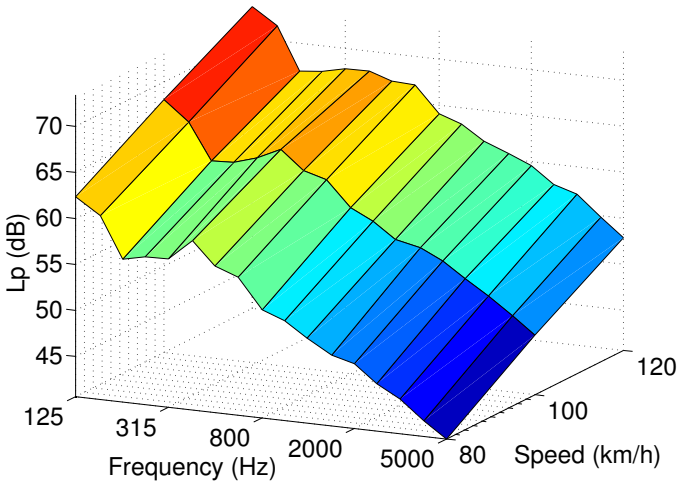

Figure 4.1: Wind tunnel measurement results as a function of frequency, at three wind velocities. The data are extracted from [7].

Slick tyres on roads with a broad roughness spectrum were investigated to fulfil the requirement of an even pitch distribution for our analysis approach. An additional requirement of the measurement data is a sufficiently high signal-to-noise ratio of the tyre/road noise compared with the vehicle wind noise. In practice this drastically reduces the number of Sperenberg cases where the proposed method can be applied. Many of the accessible cases are slick tyres on smooth surfaces where wind noise dominates in the lower frequency range of our interest. The main analysis is hence applied on the data from two rough road surfaces: A mastic asphalt surface with greywacke 2/5 and a stone mastic asphalt surface treated with a sharp-edged 5/8 mm coating, see Figures 4.2, 4.3 and 4.4.

4.2.2 Simulated data

The tyre/road interaction model at Chalmers, presented in Chapter 2.5 was used to simulate tyre/road noise. The road texture data used in the calculations are based on multi-track laser measurements of real road surfaces. Linear contact springs are included in the interaction model to account for small-scale road roughness. Two surfaces from the Kloosterzande test tracks [79] were investigated, a smooth road build according to ISO-10844 and a rough road with surface dressing 5/8. Their roughness amplitude spectra, seen in Figure 4.2, clearly show their different characters.

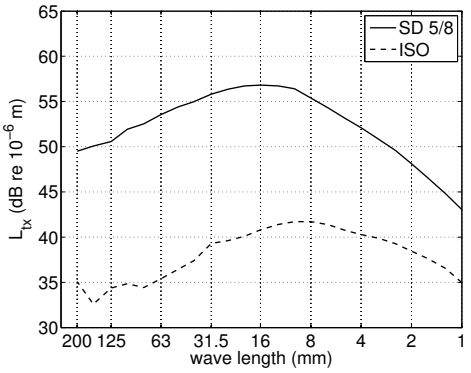

Figure 4.2: Third octave band average of the road surface spectra over all tracks and positions on the test tracks for the two simulated cases: a rough road with surface dressing 5/8 and a smooth road build according to ISO-10844.

The upper limit of the frequency range in the tyre/road interaction model is proportional to the spatial resolution and driving speed; very high frequency noise cannot be calculated for low speeds without increasing the resolution. The spatial resolution was here kept constant with 512 elements along the circumference of the tyre. Contact spring stiffness was set to 50 kN/m and even though possible, spring damping was not implemented in the contact model. Speeds between 40 and 100 km/h were used to create data sets similar to the measurements. Calculated sound pressure levels are shown up to the third octave band of 1600 Hz due to the frequency limitation for low speeds.

4.3 Result and Discussion

4.3.1 Analysis of measurement data

Coast-by measurements from two rough road surfaces are analysed here: GA1 refers to a mastic asphalt surface (Gussasphalt) 0/11 with greywacke 2/5, see Figure 4.3. A20 refers to a stone mastic asphalt 0/8 treated with a sharp edged 5/8 mm coating, see Figures 4.4 and 4.5 for the roughness spectrum of A20. Two different slick tyres were used during the measurements: DB1 is the Continental 195/65-R15 91V model mounted on the Mercedes and VW1 is the 175/70-R13 82T model mounted on the Volkswagen.

Figure 4.3: GA1 – Mastic asphalt (Gussasphalt) 0/11 with graywacke 2/5.

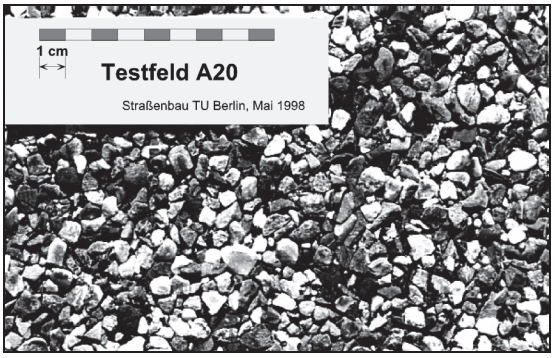

Figure 4.4: A20 – Stone mastic asphalt 0/8 with a sharp-edged 5/8 mm coating.

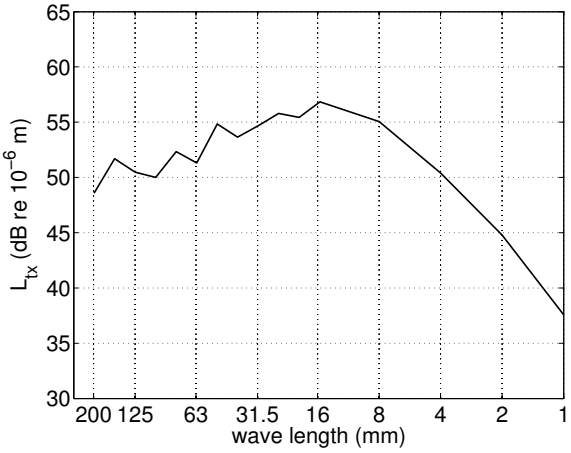

Figure 4.5: Average roughness spectrum in third octave bands of the A20 surface (stone mastic asphalt 0/8 treated with a sharp edged 5/8 mm coating).

Figure 4.6 shows the analysis results of the case with the slick tyre DB1 on the rough mastic asphalt surface GA1. The plots illustrate the contributions of the different components to the total source strength (as defined in Equation 4.3) as a function of frequency and velocity. As expected, the U^4 term is important for the high frequencies. A surprising element, however, is its share in the complex mid frequency range starting around 400–500 Hz where all three terms are active. Figure 4.7 shows detailed results with measurement data points and the total modelled sound pressure level (using Equation 4.2) including its components for separate frequency bands. The low frequencies are dominated by the U^2 term with a small contribution by the U^6 term for high speeds. As the frequency increases, U^4 grows and becomes the most important component. In the very highest frequency range, wind noise again has some influence on the data.

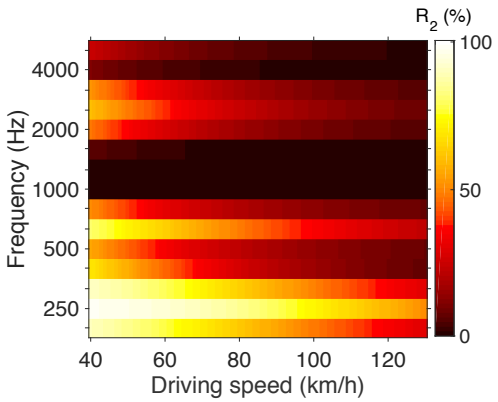

(a) Contribution of the U^2 part

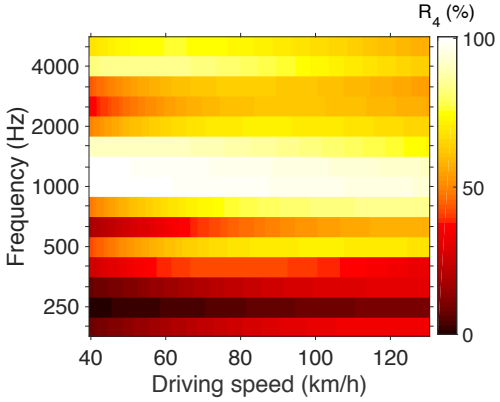

(b) Contribution of the U^4 part

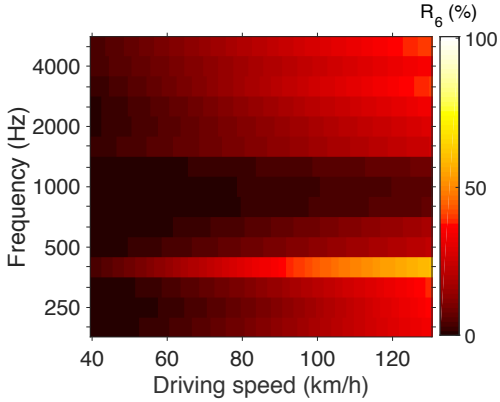

(c) Contribution of the U^6 part

Figure 4.6: Contributions of the different source components to the total modelled source strength (see Equation 4.3) for the road GA1 with the slick tyre DB1.

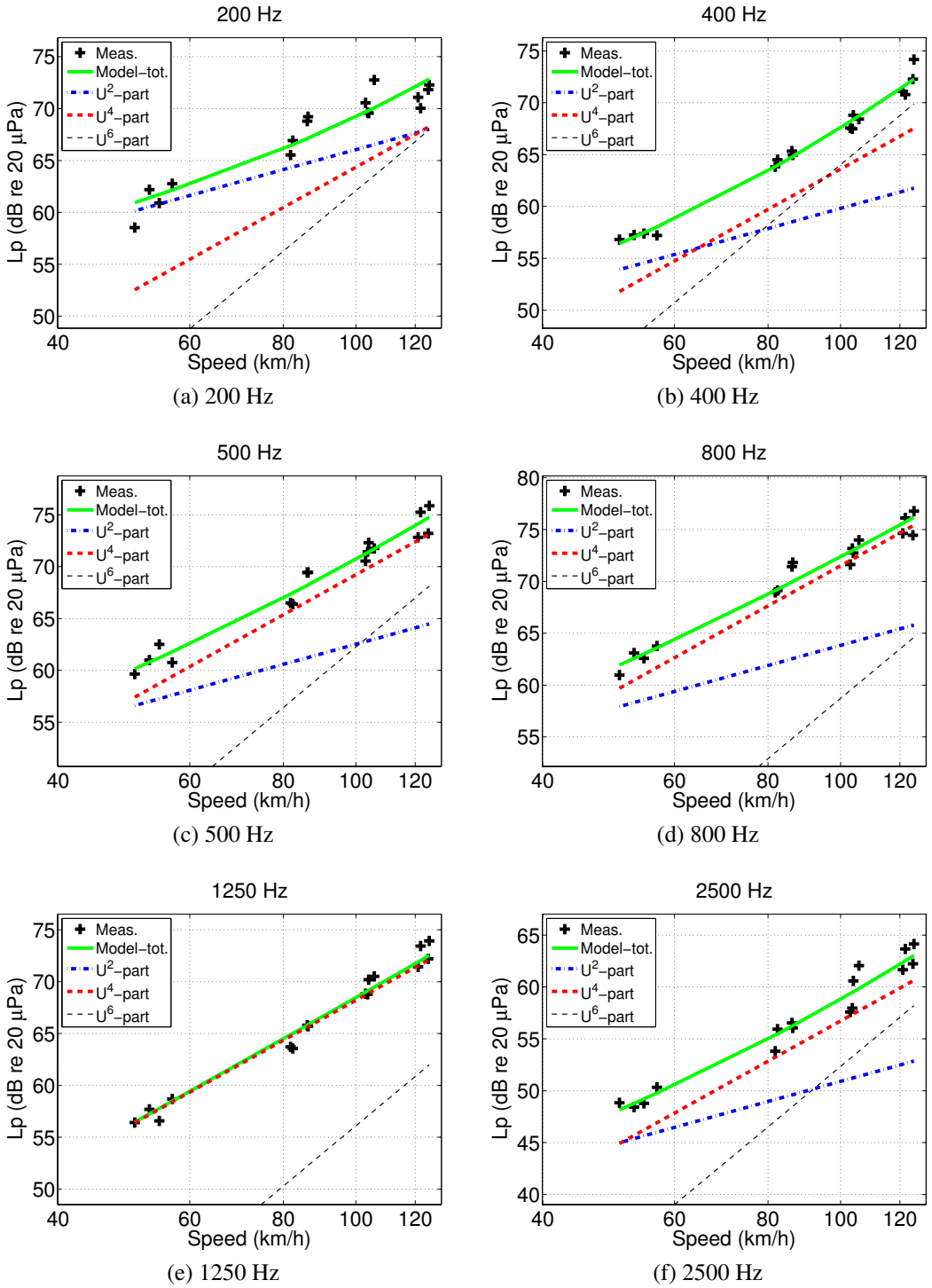

(a) 200 Hz (b) 400 Hz

(c) 500 Hz (d) 800 Hz

(e) 1250 Hz (f) 2500 Hz

Figure 4.7: Measurement data points and analysis results with the total modelled sound pressure level including its components. Examples of individual third-octave band results for the road GA1 with the tyre DB1.

Figures 4.8 and 4.9 show the contributions of the U^4 and U^2 components to the total source strength for two measurements on the rough stone mastic asphalt road surface A20 with the two different slick tyres DB1 and VW1. The U^4 component starts to become important around 400–500 Hz and dominates roughly from 800 Hz. Low speeds and frequencies in the low–mid range are dominated by the U^2 term. The residual wind noise is only noticeable in the very highest frequency bands (not shown in the figures).

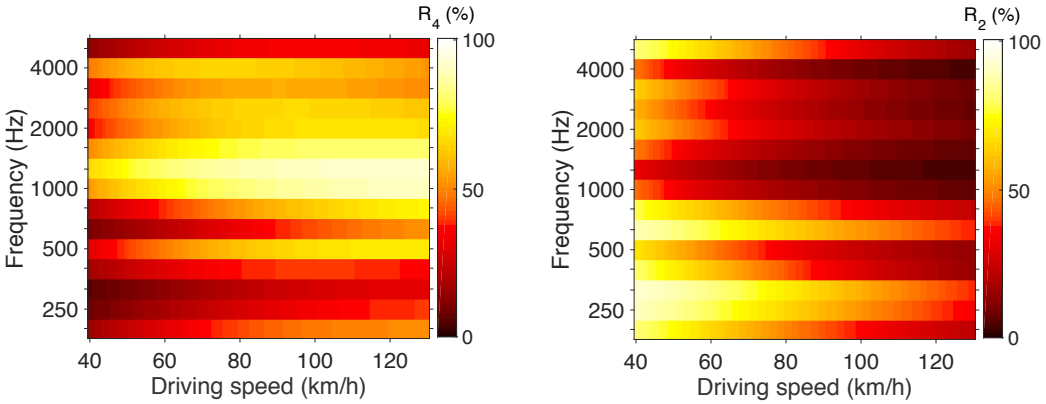

(a) Contribution of the U^4 part

(b) Contribution of the U^2 part

Figure 4.8: Contributions of the different source components to the total modelled source strength for the stone mastic asphalt surface A20 with the slick tyre DB1.

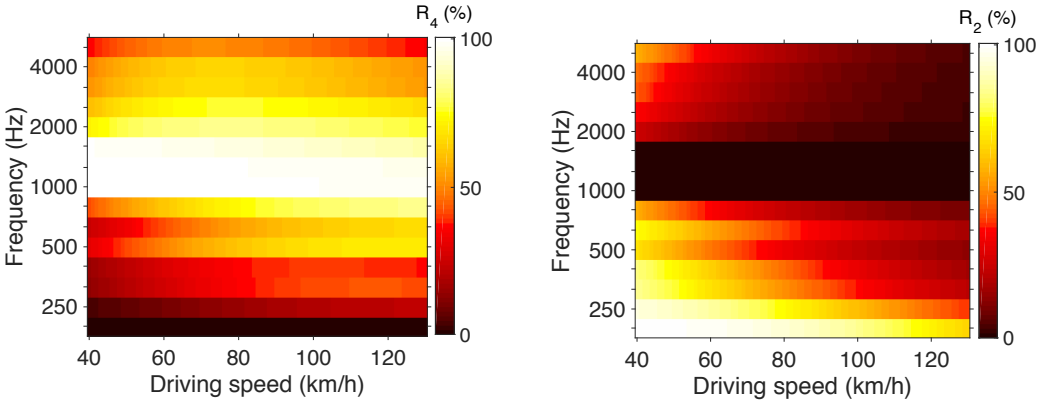

(a) Contribution of the U^4 part

(b) Contribution of the U^2 part

Figure 4.9: Contributions of the different source components to the total modelled source strength for the stone mastic asphalt surface A20 with the slick tyre VW1.

Pitch effects

Tonal tyre/road noise components, pitch effects, can be caused by regularities in e.g. the tread pattern. The frequency of the noise generated from such type of repeated event will increase with rolling speed and may disturb the speed exponent analysis of individual frequency bands. Pitch effects are especially pronounced on smooth surfaces and a speed exponent analysis in third-octave bands of such cases must be considered with care.

An example of clear pitch-related problems when studying the speed exponent is found in the case of the patterned tyre VW4 (Goodyear GEStrO-92 CLUB 175/70-R13 82T mounted on the Volkswagen) on the smooth sandpapered concrete surface B02 (Figure 4.10). Figure 4.11 shows some especially troublesome third-octave band results of the analysis. Below the 400 Hz band, the main component is wind noise but for the next frequency bands there is a large spread in the data points and only weak, if any, increase of the sound pressure level with speed. The spread of the data decreases for higher frequencies, but even around 1250 Hz there is still a waviness to the development with speed. The linear speed exponent k (see Equation 2.4) for each frequency band is also indicated to the lower right in the figures. These are gathered and displayed as a function of frequency in Figure 4.12 together with the results from the same tyre on the rough GA1 road. The big dip that is seen in the mid-frequencies for the smooth road almost vanished in the case of the rough road. The roughness of the road randomises the contact and decreases the influence of the tread pattern pitch.

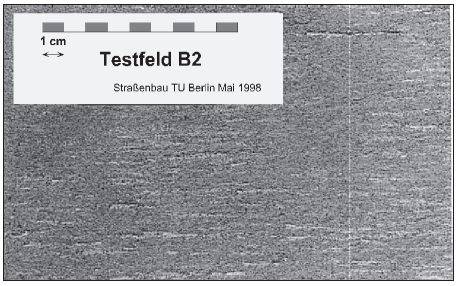

Figure 4.10: B02 – sandpapered concrete surface B02.

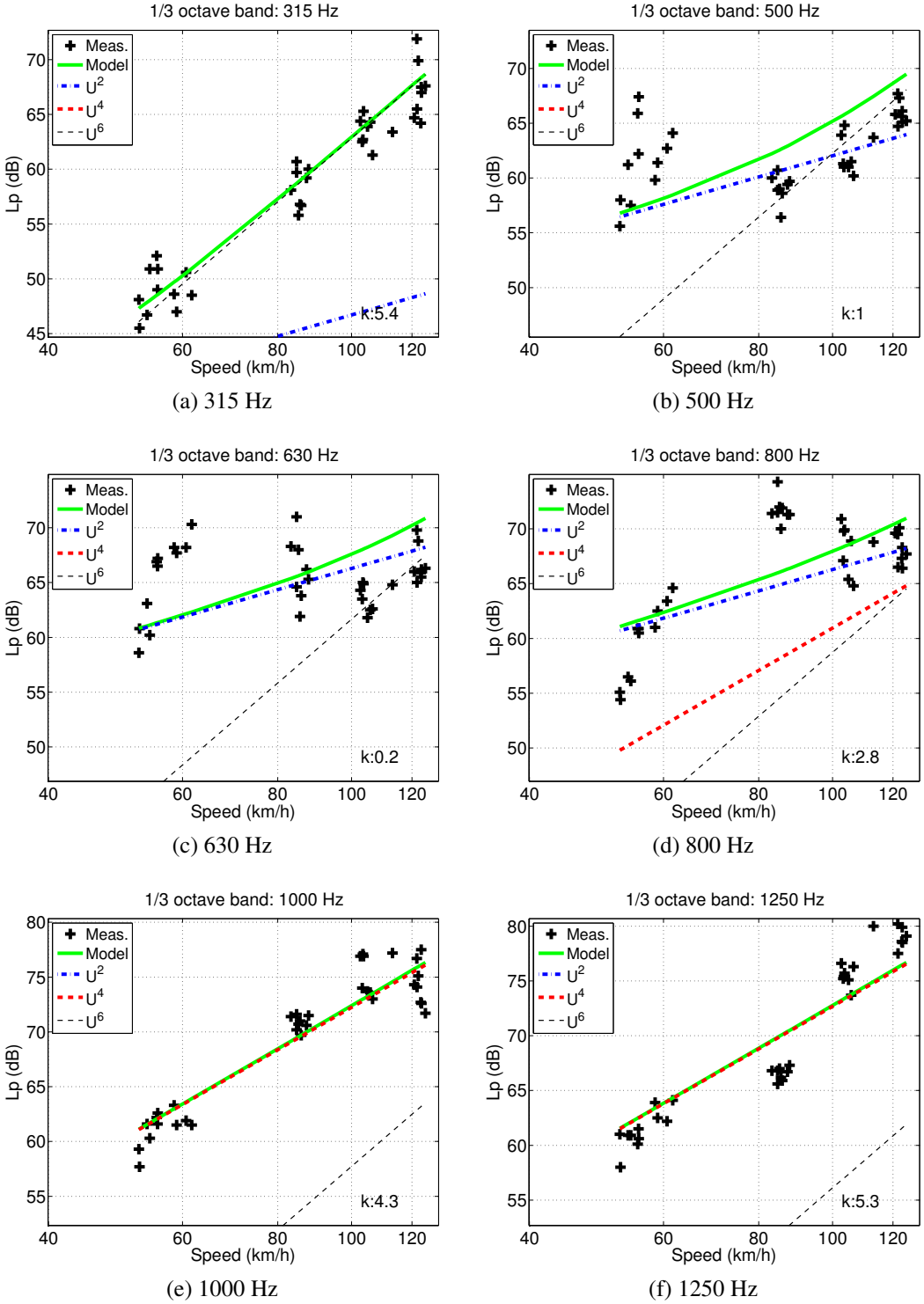

Figure 4.11: Measurement data points and analysis results with the total modelled sound pressure level including its components. Examples of individual third-octave band results for the sandpapered concrete road B02 with the patterned tyre VW4.

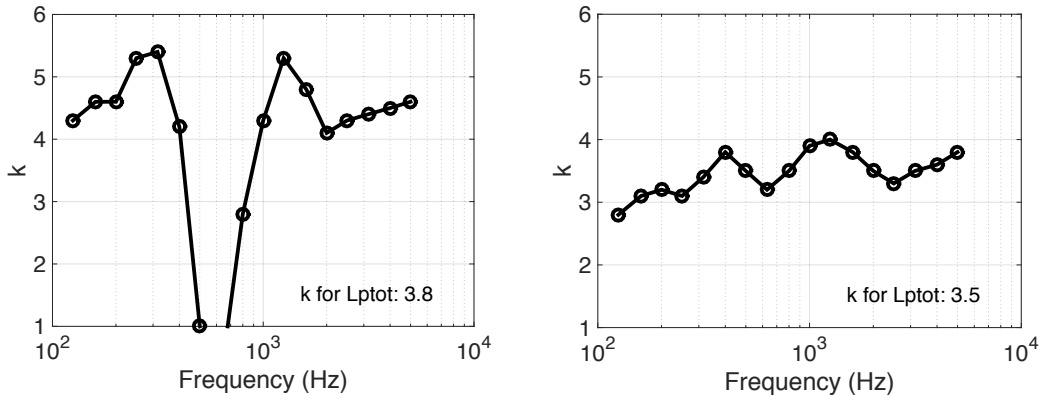

(a) VW4 B02 (b) VW4 GA1

Figure 4.12: Linear speed exponent of the third octave band results for the patterned tyre VW4 on the (a) smooth sandpapered concrete road B02 and (b) rough GA1.

Another example in which the effect of tread pattern pitch decreases is the rough mastic asphalt road surface A20 with the patterned tyre DB3. DB3 is a Continental SportContact CH90 195/65-R15 90H mounted on the Mercedes; its pattern is pictured in Figure 4.13. The linear speed exponent has a slight increase over frequency and no sign of pitch problems, see Figure 4.14. Figure 4.15 shows the results of the speed exponent analysis using Equation 4.2. The contributions of the U^4 and U^2 terms indicate similar trends as in the case with a slick tyre on the same surface, see Figures 4.8 and 4.9. The main difference is that the U^4 term is focused around the 1000 Hz band for the patterned tyre and there is also a clearer transition from U^2 for low velocities to U^4 for higher velocities, something which is seen in general for the studied cases with patterned tyres on rough roads.

Figure 4.13: Tread pattern of DB3 – Continental SportContact CH90 195/65-R15 90H mounted on the Mercedes during the measurements.

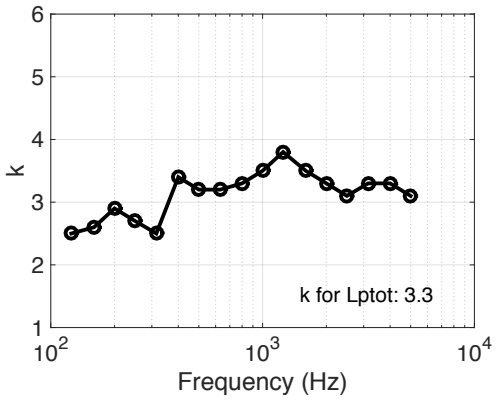

Figure 4.14: Linear speed exponent of the third-octave band results of the rough stone mastic asphalt road surface A20 with the patterned tyre DB3.

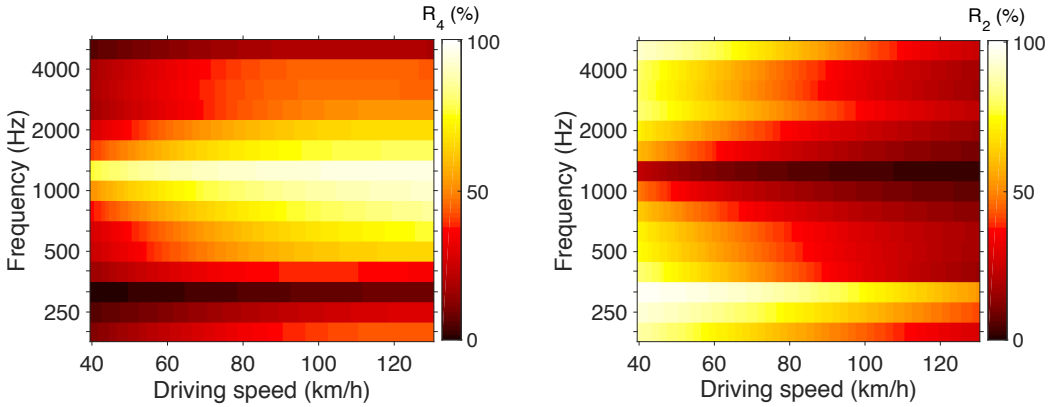

(a) (b)

Figure 4.15: Rough stone mastic asphalt road surface A20 with the patterned tyre DB3, percentage of: (a) the U^4 contribution to the total modelled source strength, (b) the U^2 contribution to the total modelled source strength.

4.3.2 Analysis of simulated data

The calculated tyre/road noise is assumed to consist of only two parts, the U^2 and the U^4 terms, as wind is not included in the model. Hence, the last term in Equation 4.2 is left out when modelling the sound pressure level and the index m in Equation 4.3 is reduced to $m = 2, 4$. Analysis results are presented in Figure 4.16 which shows that there is a U^4 component in the calculated noise and that this is mainly found in the case of the rough road. Detailed third-octave band results for the rough road are found in Figure 4.17 and for the smooth road in Figure 4.18.

The contact force spectrum (considering the sum of all contact forces at each point in time) is also analysed in a preliminary extension of the speed exponent approach. Figure 4.19 shows the simulated contact force level and sound pressure level as a function of speed for the 400 Hz third-octave band. The force level clearly grows with speed by a power of four for this case, and the sound pressure demonstrates comparable behaviour.

The tendencies are similar when studying other calculated cases resulting in the conclusion that noise from tyre vibrations induced by rolling can have a variety of speed exponents, some of which extend into what has classically been interpreted as air-pumping. It is also suggested that the contact force, at least when studied as the sum of all forces in the contact patch, has a similar speed dependency.

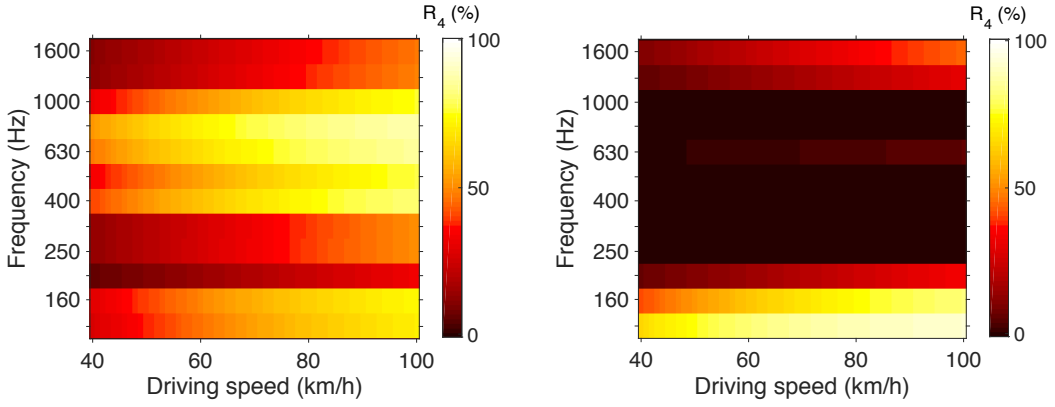

Figure 4.16: Percentage of the U^4 contribution to the total modelled source strength for the simulated cases of a slick tyre on (a) a rough surface (surface dressing 5/8) and (b) a smooth surface (ISO-10844)

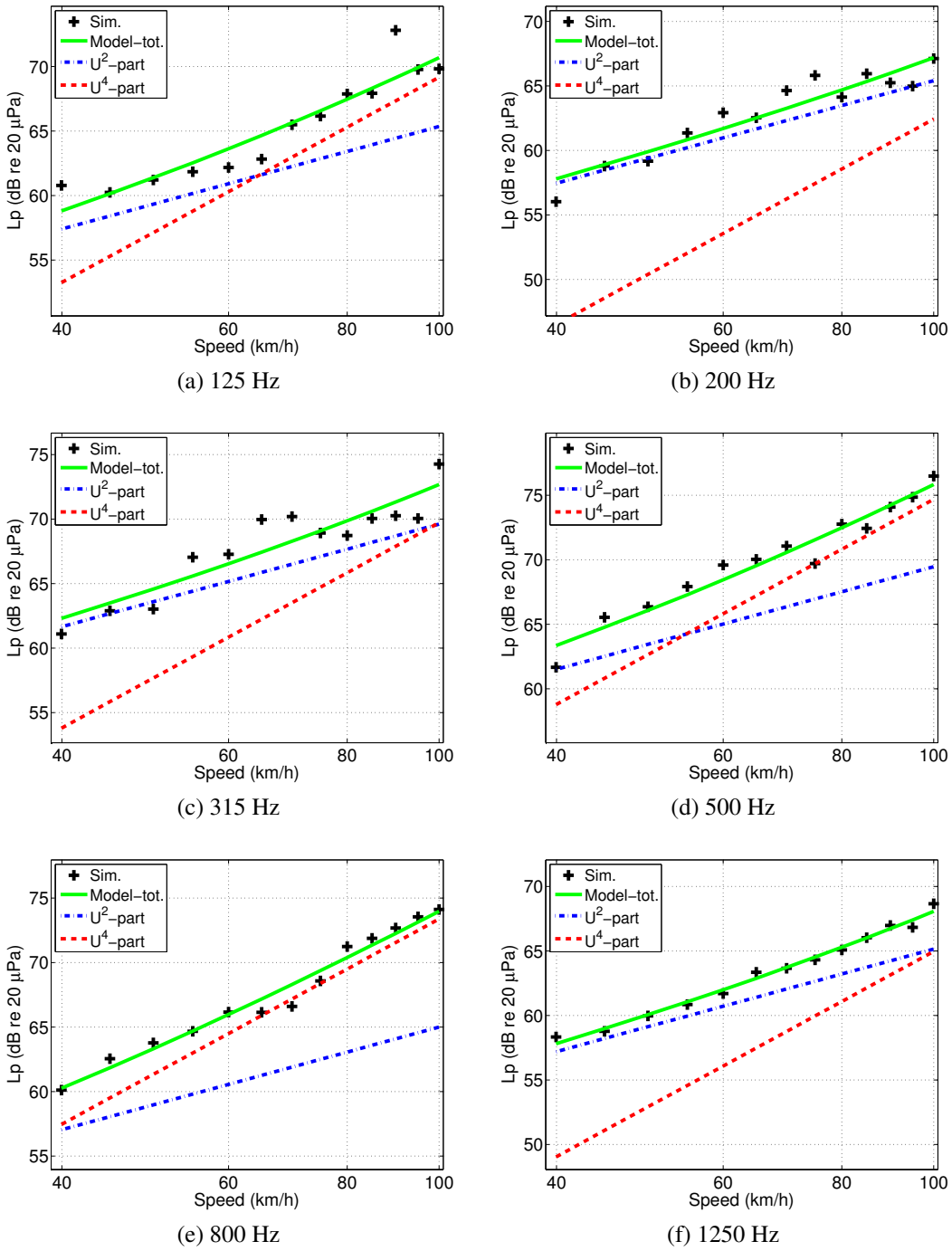

(a) 125 Hz (b) 200 Hz

(c) 315 Hz (d) 500 Hz

(e) 800 Hz (f) 1250 Hz

Figure 4.17: Simulated data points and analysis results with the total modelled sound pressure level including its components. Examples of individual third-octave band results for the simulated case of a slick tyre on a rough road (surface dressing 5/8).

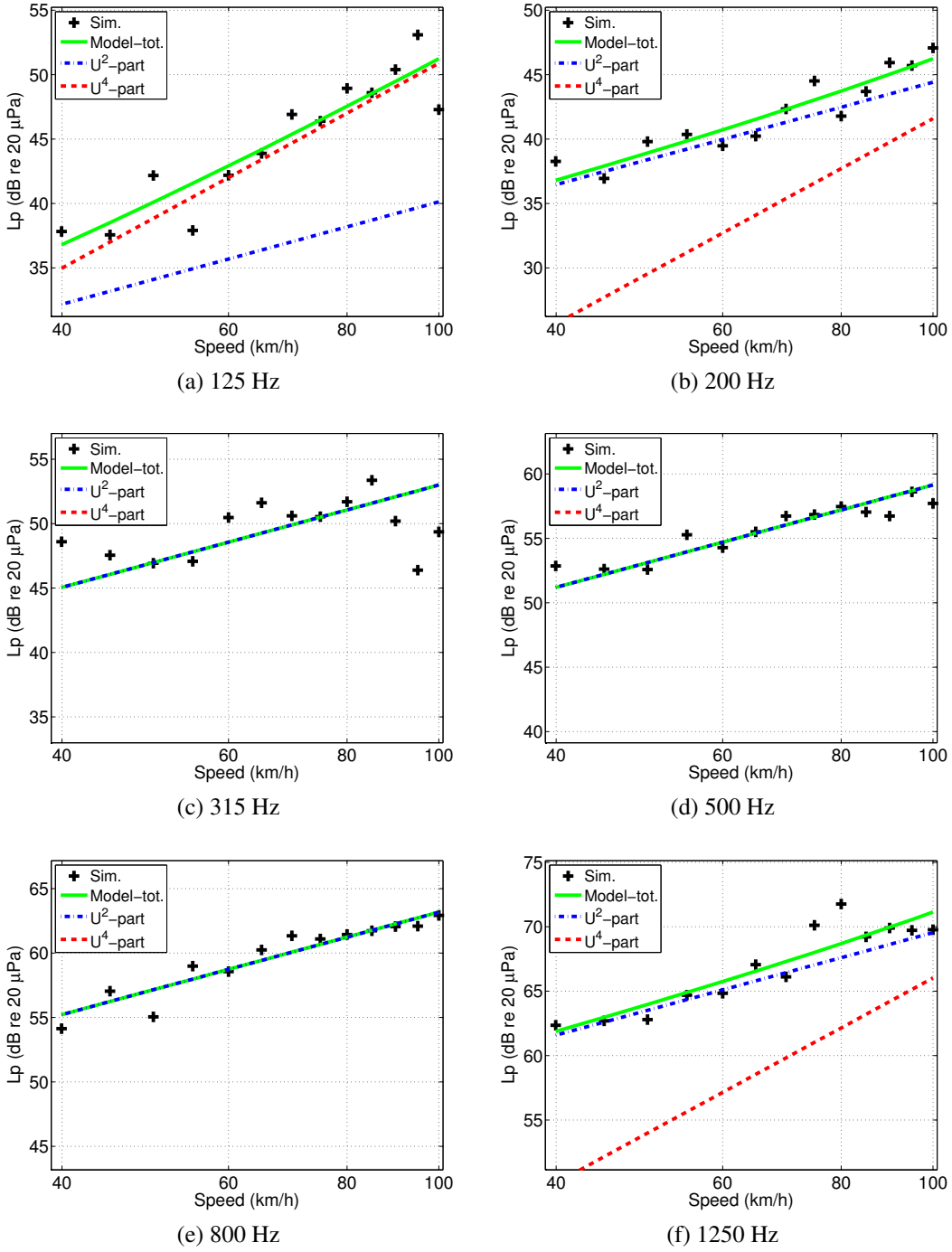

(a) 125 Hz (b) 200 Hz

(c) 315 Hz (d) 500 Hz

(e) 800 Hz (f) 1250 Hz

Figure 4.18: Simulated data points and analysis results with the total modelled sound pressure level including its components. Examples of individual third-octave band results for the simulated case of a slick tyre on a smooth surface (ISO-10844).

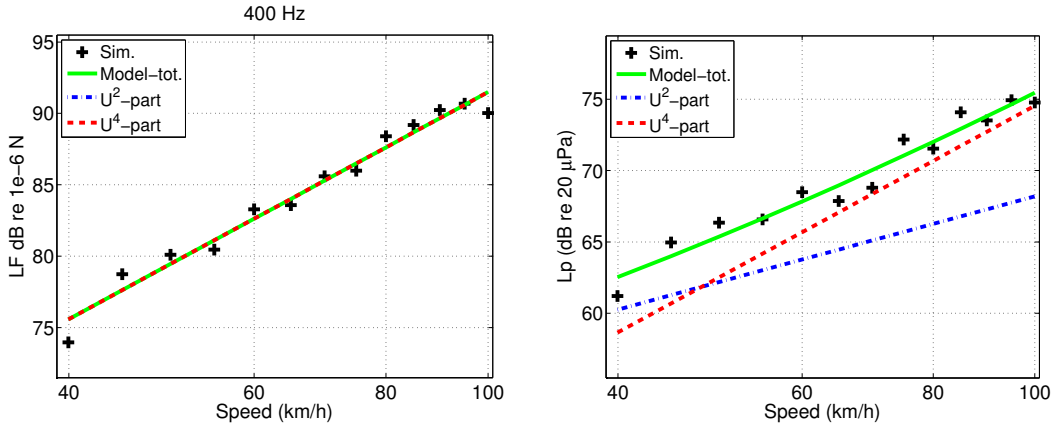

(a) LF (b) Lp

Figure 4.19: Simulated data points and speed exponent analysis results for the 400 Hz band with the modelled: (a) contact force level and (b) sound pressure level for the case of a slick tyre on a rough road (surface dressing 5/8).

4.3.3 Discussion

Speed exponent analysis has traditionally been applied on the total sound pressure level which includes possible pitch related effects. This study attempts to investigate the speed dependency of third-octave band tyre/road noise. Similar approaches are found in recent publications e.g. [16, 69, 84] and there are indications that it works sufficiently well. Compare e.g. Figure 4.20 where the speed exponent analysis is applied on the total level for measurements of the slick tyre DB1 on road surface GA1, with the third-octave band behaviour in Figures 4.6 and 4.7. Both approaches show that the U^4 component is important and cannot be omitted.

However, A-weighting might cause unnecessary uncertainties when applying a speed exponent analysis on total levels. A brief preliminary study on the cases included in this work shows that A-weighting for some cases affects the linear speed exponent of the total level. For example, the case with clear pitch related effect: the patterned tyre VW4 on the smooth sandpapered surface B02 has a different total speed exponent when A-weighting is applied than when it isn't (dB: k=4.1 dBA: k=3.8). The same tyre on the rough road GA1 shows a slight decrease of this difference (dB: k=3.5 dBA: k=3.7). Other tyre/road combinations are not this sensitive to A-weighting with respect to the linear speed exponent of the total level.

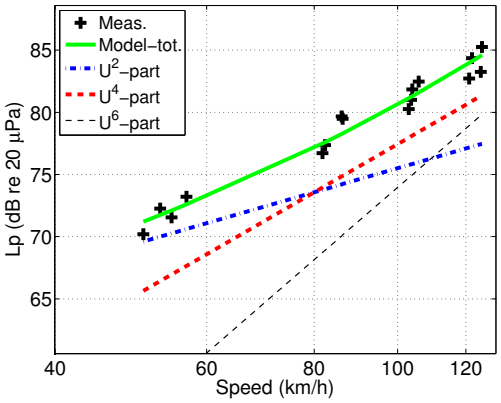

Figure 4.20: Total sound pressure level as a function of speed for the case of a slick tyre DB1 on the road surface GA1. Measurement data points and analysis results with the total modelled sound pressure level including its components.

Finding a strong U^4 component in the noise from rough road surfaces, both in measurements and simulations, is interesting, as these are typically assumed to generate noise mainly by tyre vibrations. The brief comparison with the speed dependency of the total contact force suggests a connection. To complete the picture, other surfaces should also be analysed, especially roads that are expected to generate significant air-pumping noise, such as sealed smooth surfaces and smooth surfaces with controlled cavities.

However, a speed exponent analysis requires that the contribution from vehicle wind noise, the U^6 component, is known and/or negligible. Comparing the coast-by and wind tunnel measurement data from Sperenberg indicates a domination and sometimes an overestimation of wind noise for quiet tyre/road combinations, i.e. slick tyres on smooth road surfaces [7]. A speed exponent analysis of these cases becomes very uncertain and quiet tyre/road combinations are hence excluded from our investigation. The consequence of overestimating the contribution from wind noise in the analysed cases is mainly a decrease in the contribution of the U^4 term, the conclusions concerning the presence of the U^4 contribution should still be valid.

4.4 Conclusions

A speed exponent analysis was used in this study to extract noise generation mechanisms with different speed exponents from measured and simulated tyre/road noise. The initial suggestion was that noise from tyre vibrations and noise from air-pumping mechanisms grow with speed by the powers of two and four, respectively.

An important component of U^4 is found in measured tyre/road noise on rough road surfaces, where it is expected that the noise is mainly generated by tyre vibrations, not air-pumping. The U^4 component appears in the mid-frequency spectrum, around 400–500 Hz and influences the noise up to very high frequencies. Simulated tyre/road noise also shows an important contribution of U^4, especially for rough road surfaces. This occurs even if no aerodynamic sources are included, only tyre vibrations due to rolling generate noise in the model. This leads to the conclusion that noise from tyre vibrations can grow faster with speed than what has typically been assumed. This study showed that the expected U^2 dependency is insufficient, a variety of speed exponents for tyre vibration-induced noise is found. It is also shown that tyre vibrations contribute to high-frequency tyre/road noise, giving reasons to discuss the classical division that "low-frequency noise is due to tyre vibrations and high-frequency noise is caused by air-pumping".

The discouraging conclusion concerning air-pumping is that we still do not know its significance to tyre/road noise in authentic situations. The overlap with speed exponents from tyre vibrations makes it unfeasible to separate noise created by tyre vibrations from noise created by air-pumping with a speed exponent analysis.

Chapter 5
Conclusions and future work

Tyre/road noise is a serious environmental problem and the present work has focused on the development of accurate prediction tools which simulates tyre/road noise. To do so requires an indepth understanding of the generation mechanisms causing the noise, as well as a high degree of control in the physical tyre/road noise model that is used.

Steps were taken to understand the effects of the contact stiffness formulation when modelling tyre/road noise.

In Chapter 3.1 and Paper III, a numerical tyre/road noise simulation tool based on physical relationships was used to investigate how the stiffness of the contact springs affected simulated tyre/road noise. It was found that stiffness had a significant impact on the modelled noise and that this sensitivity was mainly caused by variations in the total contact force that excites tyre vibrations. Increased contact stiffness led to increased total contact force level and a close relationship was found between total contact force and simulated sound pressure.

In Chapter 3.2 and in Paper III, the contact model in the tyre/road simulation tool was extended to include non-linear contact springs whose stiffness grew with spring deformation. Using a non-linear formulation of the springs reduced the high-frequency content in the contact forces and the generated noise, compared with cases in which the spring stiffness was a constant value. The contact evolution at individual contact points revealed that non-linear stiffness resulted in a more gradual development of the contact force, and therefore the spectrum decays faster with frequency at higher frequencies.

Dynamic contact stiffness of small-scale tread deformation was investigated using a numerical contact model.

The effects of tread mass and damping were studied in Chapter 3.3 and Paper I by simulating the detailed contact between an elastic layer and a rough road surface

using a numerical time-domain contact model. The dynamic case, with an elastic-layer impulse response that extends in time, was compared with the case with the corresponding quasi-static response. Contact stiffness increased during the indentation process as expected, and the stiffness-indentation relationship additionally depended on how rapidly the contact developed – a faster process created a stiffer contact. Material properties also altered the contact development; energy losses in the elastic layer led to significantly stiffer contact compared with the quasi-static case, and material density resulted in small ripples on the stiffness function during the initial indentation. The results imply that dynamic properties of the local tread deformation may be of importance when simulating contact details in normal tyre/road interaction conditions, but that effects of damping could, as an initial approximation, be included as increased stiffness in a quasi-static tread model.

This work includes an attempt to understand the importance of air-pumping relative to other generation mechanisms of tyre/road noise.

In Chapter 4 and Paper II, a speed exponent analysis was used to extract noise generation mechanisms with different speed exponents from measured and simulated tyre/road noise. The initial hypothesis included the theory that noise from air-pumping grows by the speed to the power of four and noise from tyre vibrations grows by the speed to the power of two. However, the latter had to be revised, as simulated rolling noise solely due to tyre vibrations showed a variety of speed exponents, of which some extended into what has classically been interpreted as air-pumping. An important component that grew by the speed to the power of four was also found in measured tyre/road noise on rough road surfaces where it is expected that the noise is mainly generated by tyre vibrations, not air-pumping. It was concluded that the overlap with speed exponents from tyre vibrations makes it unfeasible to separate noise created by tyre vibrations from noise created by air-pumping with a speed exponent analysis.

The most important contribution of the present work is an increased understanding of how the contact-spring formulation affects the simulated noise. The work also provided insights into the speed dependency of tyre/road noise generation mechanisms.

Future work

Non-linear contact stiffness formulations in tyre/road contact can be found in several experimental, numerical, and theoretical studies in the literature. The present

work has taken an initial step to include this knowledge in a full-scale tyre/road noise model. However, the stiffness functions used here are preliminary; the ideal formulation that accurately describes the contact process is still to be found and implemented in a tyre/road noise simulation tool.

The purpose of the contact springs is to include the effects of roughness on length scales smaller than the spatial resolution. By using springs with identical stiffness functions, an assumption is made that it is enough to treat roughness on these length scales with an average stiffness function. A similar approach to road roughness on larger length scales has been shown to be insufficient when modelling tyre/road noise; see e.g. Hoever in [77], in general 5–6 tracks of individual roughness data are necessary. A straight-forward extension of the present work could be to include a variation of the contact springs. This could e.g. perturb the contact resonance phenomena, seen especially in the results on the smoother road in Chapter 3.2.2.

Another extension of the present work could be to investigate whether including energy losses in the contact spring formulation could reduce the contact resonance phenomena. It would also be interesting to see if a higher degree of asymmetry would be obtained in the time evolution at individual contact points if damping was included in the small-scale contact as found by Zhang [20], among others. Damping in the tread material was found to increase the effective contact stiffness in the detailed tread/road contact model used in Chapter 3.3 and Paper I. The stiffness also depended on how fast the contact developed, and it was suggested that damping could be approximated using a stiffening factor, possibly linked to the rolling speed. It would be interesting to implement such a dependency and e.g. study how it affects the speed exponent of simulated tyre/road noise.

The present work concluded that the presence of air-pumping can unfortunately not be investigated using a speed exponent analysis. Hence the question remains: Why do we have such a good resemblance between measured and simulated high-frequency tyre/road noise when the latter only includes the contribution from tyre vibrations? Either real-world tyre/road noise is really dominated by tyre vibrations that the model correctly captures. However, the present study opens up for another explanation – that the high-frequency content of the modelled tyre/road noise might be overestimated when using contact springs with constant stiffness. Using non-linear springs reduced the high-frequency content, which implies less good agreement with measured data. It does not, however, mean that air-pumping is responsible for the difference between measurements and simulations. For example, adhesive forces could lead to stick-snap behaviour of the tread, which in turn may generate high-frequency noise. Adhesive forces should be feasible to implement in the present contact model; even if this would add complexity to the model, it might give valuable insights.

Bibliography

[1] L. Fritschi, A. L. Brown, R. Kim, D. Schwela, and S. Kephalopoulos. *Burden of disease from environmental noise – Quantification of healthy life years lost in Europe*. World Health Organization – Regional Office for Europe, Platz der Vereinten Nationen 1, Bonn, Germany, 2011.

[2] C. Nugent, N. Blanes, J. Fons, M. Sáinz de la Maza, M. J. Ramos, F. Domingues, A. van Beek, and D. Houthuijs. *Noise in Europe 2014*. Number 10/2014. European Environment Agency, Publications Office of the European Union, Luxembourg, Dec 2014.

[3] B. Berglund, T. Lindvall, and D. H. Schwela. *Guidelines for Community noise*. World Health Organization, Geneva, 1999.

[4] *Night noise guidelines for Europe*. World Health Organization, Regional Office for Europe European Centre for Environment and Health, Bonn, Germany, 2009.

[5] U. Sandberg and J. Ejsmont. *Tyre/road noise reference book*. Informex, Kisa, Sweden, 2002.

[6] W. van Keulen and M. Duškov. Inventory study of basic knowledge on tyre/road noise. Technical Report DWW-2005-022, The Dutch Innovation Programme on noise mitigation, IPG, 2005.

[7] T. Beckenbauer. Effect of pavement texture on tyre/pavement noise (orig. Einfluss der Fahrbahntextur auf das Reifen-Fahrbahn-Geräusch). Scientific report FE 03.293/1995/MRB, German Federal Ministry of Transport, Buildings and Dwellings, Bonn, Germany, 2001.

[8] P. B. U Andersson and W. Kropp. Rapid tyre/road separation: An experimental study of adherence forces and noise generation. *Wear*, 266(1-2):129–138, 2009.

[9] O. E. Lundberg, I. Lopez Arteaga, and L. Kari. Experimental study of the rolling contact forces between a tyre tread-block and a road. In *Proceedings of Inter Noise 2016, Hamburg, Germany*, pages 2179–2184, Aug 2016.

[10] D. Ronneberger. Towards quantitative prediction of tyre/road noise. In *Proceedings of the Workshop on rolling noise generation, Berlin*, pages 218–235, 1989.

[11] R.A.G Graf, C.-Y. Kuo, A. P. Dowling, and W. R. Graham. On the horn effect of a tyre/road interface, part i: Experiment and computation. *Journal of Sound and Vibration*, 256(3):417–431, 2002.

[12] W. Kropp, F.-X. Bécot, and S. Barrelet. On the sound radiation from tyres. *Acta Acust United Ac*, 86(5):769–779, Jan 2000.

[13] B. Wang and D. Duhamel. On the design and optimization of acoustic network resonators for tire/road noise reduction. *Applied Acoustics*, 120:75–84, Jan 2017.

[14] A. Kuijpers, H.M. Peeters, W. Kropp, and T. Beckenbauer. ACOUSTIC OPTIMIZATION TOOL: RE4 – modeling refinements in the SPERoN framework. Technical Report M+P.DWW.06.04.7, Ministerie van V&W, DVS, the Netherlands, Nov 2007.

[15] S. Alves and M. Männel. Application of SPERoN to the develompent of low noise road surfaces. *Proceedings of EuroRegio 2016 Porto, Portugal*, May 2016.

[16] G. Dubois, J. Cesbron, H. P. Yin, F. Anfosso-Lédée, and D. Duhamel. Statistical estimation of low frequency tyre/road noise from numerical contact forces. *Applied Acoustics*, 74(9):1085–1093, 2013.

[17] G. Dubois, J. Cesbron, H. P. Yin, and F. Anfosso-Lédée. Numerical evaluation of tyre/road contact pressures using a multi-asperity approach. *International Journal of Mechanical Sciences*, 54(1):84–94, 2012.

[18] O. E. Lundberg. *On the influence of surface roughness on rolling contact forces*. PhD thesis, KTH, Aeronautical and Vehicle Engineering, Marcus Wallenberg Laboratory MWL, Stockholm, Sweden, Nov 2016.

[19] F. Liu, M. P. F. Sutcliffe, and W. R. Graham. Prediction of tread block forces for a free-rolling tyre in contact with a smooth road. *Wear*, 269(9-10):672–683, 2010.

[20] Y. Zhang. *Study on a test rig of dynamic tyre/road contact forces at the origin of rolling noise*. PhD thesis, IFSTTAR, Centrale Nantes, France, Sep 2016.

[21] J. Cesbron, F. Anfosso-Lédée, D. Duhamel, H. P. Yin, and D. Le Houédec. Experimental study of tyre/road contact forces in rolling conditions for noise prediction. *Journal of Sound and Vibration*, 230:125–144, 2009.

[22] F. Wullens and W. Kropp. A three-dimensional contact model for tyre/road interaction in rolling conditions. *Acta Acustica united with Acustica*, 90(4):702–711, 2004.

[23] W. Kropp. Structure-borne sound on a smooth tyre. *Applied Acoustics*, 26(3):181–192, Jan 1989.

[24] P. B. U. Andersson, K. Larsson, F. Wullens, and W. Kropp. High frequency dynamic behaviour of smooth and patterned passenger car tyres. *Acta Acustica united with Acustica*, 90:445–456, 2004.

[25] K. Larsson and W. Kropp. A high-frequency three-dimensional tyre model based on two coupled elastic layers. *Journal of Sound and Vibration*, 253(4):889–908, 2002.

[26] C. Hoever. *The simulation of car and truck tyre vibrations, rolling resistance and rolling noise*. PhD thesis, Division of Applied Acoustics, Chalmers University of Technology, 2014.

[27] M. Brinkmeier, U. Nackenhorst, S. Petersen, and O. von Estorff. A finite element approach for the simulation of tire rolling noise. *Journal of Sound and Vibration*, 309(1-2):20–39, 2008.

[28] Y. Waki, B. R. Mace, and M. J. Brennan. Free and forced vibrations of a tyre using a wave/finite element approach. *Journal of Sound and Vibration*, 323(3-5):737–756, 2009.

[29] A. Fadavi, D. Duhamel, and H. P. Yin. Tyre/road noise: Finite element modeling of tyre vibrations. In *Proceedings of Internoise 2001, The Hague, The Netherlands*, The Hague, The Netherlands, 2001.

[30] I. Lopez Arteaga. Green's functions for a loaded rolling tyre. *International Journal of Solids and Structures*, 48(25):3462–3470, 2011.

[31] C.-M. Nilsson. *Waveguide finite elements applied on a car tyre*. PhD thesis, Department of Aeronautical and Vehicle Technology, Royal Institute of Technology, Stockholm, Sweden, 2004.

[32] S. Finnveden and M. Fraggstedt. Waveguide finite elements for curved structures. *Journal of Sound and Vibration*, 312(4-5):644–671, Jan 2008.

[33] M. Fraggstedt. *Vibrations, damping and power dissipation in Car Tyres*. PhD thesis, Royal Institute of Technology, Department of Aeronautical and Vehicle Engineering, Stockholm, Sweden, May 2008.

[34] P. Sabiniarz. *Modelling the vibrations on a rolling tyre and their relation to exterior and interior noise*. PhD thesis, Division of Applied Acoustics, Chalmers University of Technology, Göteborg, 2011.

[35] W. Kropp, P. Sabiniarz, H. Brick, and T. Beckenbauer. On the sound radiation of a rolling tyre. *Journal of Sound and Vibration*, 331(8):1789 – 1805, 2012.

[36] W. Kropp. *Ein Modell zur Beschreibung des Rollgeräusches eines unprofilierten Gürtelreifens auf rauher Strassenoberfläche, (A model for the description of the rolling noise from a smooth tyre on a rough road)*. PhD thesis, Fortschritt-Berichte Reihe 11, Nr 166, VDI Verlag, Düsseldorf, 1992.

[37] J. F. Hamet and P. H. Klein. Use of a rolling model for the study of the correlation between road texture and tire noise. In *Proceedings of Internoise 2001, The Hague, The Netherlands*, Apr 2001.

[38] D. J. O'Boy and A. P. Dowling. Tyre/road interaction noise-numerical noise prediction of a patterned tyre on a rough road surface. *Journal of Sound and Vibration*, 323(1-2):270–291, Jan 2009.

[39] C. Hoever, A. Tsotras, E.-U. Saemann, and W. Kropp. A comparison between finite element and waveguide finite element methods for the simulation of tire/road interaction. In *Proceedings of Internoise 2013, Innsbruck, Austria*, 2013.

[40] C. Hoever and W. Kropp. The simulation of truck tire rolling noise. In *Proceedings of Inter-Noise 2015, San Francisco, USA*, volume 44, pages 1834–1845, 2015.

[41] J. Cesbron, H. P. Yin, F. Anfosso-Lédée, D. Duhamel, D. Le Houédec, and Z.Q. Feng. Numerical and experimental study of multi-contact on an elastic half-space. *International Journal of Mechanical Sciences*, 51(1):33–40, 2009.

[42] Y. Zhang, J. Cesbron, H. P. Yin, and M. Bérengier. Dynamic contact law between a rolling pneumatic tyre and a single asperity. In *Proceedings of Inter Noise 2016, Hamburg, Germany*, Aug 2016.

[43] G. Dubois, J. Cesbron, H. P. Yin, and F. Anfosso-Lédée. Macro-scale approach for rough frictionless multi-indentation on a viscoelastic half-space. *Wear*, 272(1):69–78, 2011.

[44] F. Liu, M. P. F. Sutcliffe, and W. R. Graham. Prediction of tread block forces for a free-rolling tyre in contact with a rough road. *Wear*, 282-283:1–11, May 2012.

[45] C. Hoever and W. Kropp. A model for investigating the influence of road surface texture and tyre tread pattern on rolling resistance. *Journal of Sound and Vibration*, 351(C):161–176, Sep 2015.

[46] I. Lopez Arteaga. Tyre/road noise and vibration: Understanding their interaction and contribution to vehicle noise and fuel consumption. In *21st International Congress on Sound and Vibration (ICSV21) 2014, Beijing, China*, July 2014.

[47] G. Gäbel and M. Kröger. Non-linear contact stiffness in tyre-road interaction. In *Euronoise 2006, Tampere, Finland*, Mar 2006.

[48] P. B. U. Andersson and W. Kropp. Time domain contact model for tyre/road interaction including nonlinear contact stiffness due to small-scale roughness. *Journal of Sound and Vibration*, 318:296–312, 2008.

[49] S. Boere, I. Lopez Arteaga, A. Kuijpers, and H. Nijmeijer. Tyre/road interaction model for the prediction of road texture influence on rolling resistance. *International Journal of Vehicle Design*, 65(2/3):202–221, Mar 2014.

[50] B. N. J. Persson, O. Albohr, U. Tartaglino, A. I. Volokitin, and E. Tosatti. On the nature of surface roughness with application to contact mechanics, sealing, rubber friction and adhesion. *Journal Of Physics: Condensed Matter*, 17, Dec 2005.

[51] D. Wang, A. Ueckermann, A. Schacht, M. Oeser, B. Steinauer, and B. N. J. Persson. Tire–road contact stiffness. *Tribol Lett*, 56(2):397–402, Nov 2014.

[52] R. J. Pinnington. Tyre–road contact using a particle–envelope surface model. *Journal of Sound and Vibration*, 332(26):7055 – 7075, 2013.

[53] F. Wullens and W. Kropp. Influence of the local stiffness of the rubber layer of the tyre on the generation of tyre/road noise. In *Proceedings of ICA 2001 Rome, Italy*, 2001.

[54] C. Hoever. *The influence of modelling parameters on the simulation of car tyre rolling losses and rolling noise*. Lic thesis. Department of Civil and Environmental Engineering, Chalmers University of Technology, 2012.

[55] P. B. U. Andersson. *High frequency tyre vibrations*. Lic thesis. Division of Applied Acoustics, Chalmers University of Technology, Göteborg, Sweden, 2002.

[56] R. E. Hayden. Roadside noise from the interaction of a rolling tire with the road surface. In *Purdue Noise Control Conference, Purdue University, West Lafayette, USA*, pages 62–67. Acoustical Society of America, 1971.

[57] K. J. Plotkin, M. L. Montroll, and W. R. Fuller. The generation of tire noise by air pumping and carcass vibration. In *Proceedings of Inter-Noise 1980, Miami, USA*, volume 1, pages 273–276, Dec 1980.

[58] Centre Scientifique et Technique du Bâtiment (CSTB). ITARI project - deliverable 2.4 "Global model: ground+tyre+Fluent+radiation". Project no. TST3-CT-2003-506437, Aug 1 2007.

[59] J.-F. Hamet, C. Deffayet, and M.-A. Pallas. Air-pumping phenomena in road cavities. In *Proceedings of the International Tire/Road Noise Conferance 1990, Gothenburg, Sweden*, pages 19–29, Aug 1990.

[60] N.-Å. Nilsson. Air resonant and vibrational radiation - possible mechanisms for noise from cross-bar tires. In *Proceedings of the International Tire Noise Conferance 1979, Stockholm, Sweden*, pages 93–109, Aug 1979.

[61] F. Conte and P. Jean. CFD modelling of air compression and release in road cavities during tyre/road interaction. In *Proceednings of Euronoise 2006, Tampere, Finland*, 2006.

[62] F. Conte and P. Klein. 3D CFD modelling of air pumping noise from road cavities with constant volume. In *Proceednings of Inter-noise 2013, Innsbruck, Austria*, Sep 2013.

[63] F. Conte, P. Klein, and M. Bérengier. Investigating lateral porosity effect on air pumping noise from connected road cavities with CFD simulations. In *Proceedings of Inter-noise 2014, Melbourne, Australia*, Nov 2014.

[64] M. J. Gagen. Novel acoustic sources from squeezed cavities in car tires. *The Journal of the Acoustical Society of America*, 106(2):794–801, Aug 1999.

[65] S. Kim, W. Jeong, Y. Park, and S. Lee. Prediction method for tire air-pumping noise using a hybrid technique. *Journal of the Acoustical Society of America*, 119(6):3799–3812, June 2006.

[66] M. Heckl. Tyre noise generation. *Wear*, 113:157–170, 1986.

[67] F. Conte. *Modélisation CFD du phénomène acoustique de pompage d'air dans un contact pneumatique/chaussée*. PhD thesis, Institut National des Sciences Appliquées de Lyon, France, 2008.

[68] M. Heckl and H. A. Müller. *Technische Akustik*. Springer-Verlag, Berlin/Heidelberg, 1975.

[69] S. E. Paje, M. Bueno, U. Viñuela, and F. Terán. Toward the acoustical characterization of asphalt pavements: analysis of the tire/road sound from a porous surface. *Journal of the Acoustical Society of America*, 125(1):5–7, Jan 2009.

[70] L. J. Oswald. Exterior-radiated aerodynamic noise of vehicles at highway speeds. In *Proceedings of Inter-Noise 1978, San Francisco, USA*, pages 711–714, 1978.

[71] F. Anfosso-Lédée and J. Kragh. Wind noise influence on close-proximity tyre/road noise measurements with uncovered systems. In *Proceednings of Inter-noise 2013, Innsbruck, Austria*, 2013.

[72] K. Larsson. *Modelling of Dynamic Contact - Exemplified on the Tyre/Road Interaction*. PhD thesis, Division of Applied Acoustics, Chalmers University of Technology, 2002.

[73] F. Wullens. *Excitation of Tyre Vibrations due to Tyre/Road Interaction*. PhD thesis, Division of Applied Acoustics, Chalmers University of Technology, Göteborg, Sweden, 2004.

[74] P. B. U. Andersson. *Modelling Interfacial Details in Tyre/Road Contact - Adhesion Forces and Non-Linear Contact Stiffness*. PhD thesis, Division of Applied Acoustics, Chalmers University of Technology, Göteborg, Sweden, 2005.

[75] P. Sabiniarz and W. Kropp. A waveguide finite element aided analysis of the wave field on a stationary tyre, not in contact with the ground. *Journal of Sound and Vibration*, 329(15):3041–3064, 2010.

[76] C. Hoever and W. Kropp. The simulation of tyre/road interaction and exterior rolling noise for road surfaces with transversal discontinuities. In *Proceedings of Inter Noise 2016, Hamburg, Germany*, pages 2265–2276, 2016.

[77] C. Hoever and W. Kropp. The influence of lateral road surface resolution on the simulation of car tyre rolling losses and rolling noise. In *Proceedings of Inter Noise 2013, Innsbruck, Austria*, 2013.

[78] H. Brick. *Application of the Boundary Element Method to combustion noise and half-space problems*. PhD thesis, Division of Applied Acoustics, Chalmers University of Technology, 2009.

[79] W. Schwanen, H.M. van Leeuwen, and A.A.A Peeters. Acoustic optimization tool - RE3: Measurement data Kloosterzande test track. Technical Report M+P.DWW.06.04.8, Rijkswaterstaat, Dienst Verkeer en Scheepvaart, B.H.P.A.M. The, Postbus 5044, 2600 GA Delft, 2007.

[80] J. Winroth. *Dynamic contact stiffness and air-flow related source mechanisms in the tyre/road contact*. Lic thesis. Division of Applied Acoustics, Chalmers University of Technology, Göteborg, Sweden, 2013.

[81] F. Yang. Indentation of an incompressible elastic film. *Mechanics of Materials*, 30:275–286, Jan 1998.

[82] K. Larsson, S. Barrelet, and W. Kropp. The modelling of the dynamic behaviour of tyre tread blocks. *Applied Acoustics*, 63(6):659–677, 2002.

[83] A. Kuijpers. Further analysis of the sperenberg data – towards a better understanding of the processes influencing tyre/road noise. Technical Report M+P .MVM.99.3.1, Dutch ministry of Public Housing, Physical Planning and Environment (VROM), the Netherlands, Nov 2001.

[84] E. Bühlmann, U. Sandberg, and P. Mioduszewski. Speed dependency of temperature effects on road traffic noise. In *Proceedings of Inter-Noise 2015, San Francisco, USA*, 2015.